Master's thesis

NTNU
Norwegian University of Science and Technology
Faculty of Natural Sciences
Department of Chemistry

Mehdi Movahed Aagre

Assessing Root Development and Porosity in Ameliorated and Revegetated Bauxite Residue from Hydro-Alunorte, Brazil, through Digital Analysis of X-ray Micro Computed Tomography Images

Master's thesis in Environmental Chemistry
Supervisor: Hans Peter Arp
Co-supervisor: Santiago Quinteros
May 2023

NTNU
Norwegian University of Science and Technology

NGI

Mehdi Movahed Aagre

Assessing Root Development and Porosity in Ameliorated and Revegetated Bauxite Residue from Hydro-Alunorte, Brazil, through Digital Analysis of X-ray Micro Computed Tomography Images

Master's thesis in Environmental Chemistry
Supervisor: Hans Peter Arp
Co-supervisor: Santiago Quinteros
May 2023

Norwegian University of Science and Technology
Faculty of Natural Sciences
Department of Chemistry

NTNU
Norwegian University of
Science and Technology

Abstract

Bauxite residue (BR) is a highly alkaline, saline, and sodic tailing of alumina refineries with little re-use potential and is mainly dry-stacked in land disposal areas. Erosion of BR caused by wind and rain poses a risk of contamination to the surrounding aquatic and terrestrial environments. In situ revegetation of the ameliorated residue is considered an effective strategy for mitigating the environmental risks. The aim of this study was to assess the revegetation of samples from Hydro-Alunorte refinery in Brazil by focusing on the root development. Image analysis techniques were performed on micro-computed tomography (μCT) scans from 5 BR samples that were amended by different compositions of gypsum and local organic waste. The samples had been through laboratory leaching tests that mimicked the local rainfall levels and improved their overall chemical condition before plantation of ryegrass seeds. μCT scans were taken before plantation as well as after two and four weeks of grass growth. After manual segmentation of roots from the mixtures, they were quantitatively analysed by measuring the roots features typically used in geotechnical engineering when assessing vegetated soils: number and depth of roots (RD), root volume density (RVD), root area ratio (RAR), and porosity of the soil. Moreover, latent variant and clustering analysis were done on the chemical data from the samples to show the link between samples chemistry and root growth accommodation. Thirty seeds were planted in each sample and after two weeks the samples showed up to 21 roots with an average depth of 10mm. After four weeks, the samples exhibited up to 50 roots with an average depth of 12mm. RVD mean value was 0.2% after two weeks and 1% after four weeks and RAR reached up to average value of 0.4% across column depth. Porosity values across all samples averaged into 64% before plantation, 54% after two weeks, and 37% after 4 weeks of growth. The first group had 10% gypsum content with no organic waste, 5% acai seed waste, or 5% organic food waste. The second group had 5% gypsum with 5% acai seed waste, or 5% organic food waste. The first group exhibited varying degrees of root development. The sample without organic amendment displayed the highest root growth, while distinct differences were observed between the samples with acai and food waste amendments. The second group had very poor to no growth. Clustering analysis agreed with the inter- and intra-group variation in root development. A strong correlation (R^2=0.95) was found between RD and electrical conductivity (EC) and to a lesser extent (R^2=0.83) with calcium (Ca) concentration. Furthermore, RAR and RVD were negatively correlated with alkalinity with R^2 value of 0.72 and 0.64, respectively. It was concluded that digital image analysis based on μCT is an effective method to analyse the roots and porosity in bauxite residue and that root growth is significantly associated with EC, Ca concentration, and alkalinity of the mixtures. These relationships are greatly influenced by leaching procedure, weight proportion of gypsum and the type of the organic waste that is used as amendment.

Sammendrag

Bauksittrester (BR) er en svært alkalisk, saltholdig og sodisk rest av aluminaraffinerier med lite gjenbrukspotensial og er hovedsakelig tørrstablet i landdeponeringsområder. Erosjon av BR forårsaket av vind og regn utgjør en risiko for forurensning av de omkringliggende vann- og terrestriske miljøene. Revegetering på stedet av den forbedrede resten anses som en effektiv strategi for å redusere miljørisikoen. Målet med denne studien var å vurdere revegetering av prøver fra Hydro-Alunorte-raffineriet i Brasil ved å fokusere på rotutviklingen. Bildeanalyseteknikker ble utført på skanninger med mikrocomputertomografi (µCT) fra 5 BR-prøver som ble endret av forskjellige sammensetninger av gips og lokalt organisk avfall. Prøvene hadde vært gjennom laboratorietester som etterlignet de lokale nedbørsnivåene og forbedret deres generelle kjemiske tilstand før planting av raigrasfrø. µCT-skanninger ble tatt før planting samt etter to og fire uker med gressvekst. Etter manuell segmentering av røtter fra blandingene ble de kvantitativt analysert ved å måle rotegenskapene som vanligvis brukes i geoteknisk prosjektering ved vurdering av vegetert jord: antall og dybde på røtter (RD), rotvolumtetthet (RVD), rotarealforhold (RAR) og porøsitet i jorda. Dessuten ble latent variant og klyngeanalyse gjort på de kjemiske dataene fra prøvene for å vise sammenhengen mellom prøvenes kjemi og innkvartering av rotvekst. Tretti frø ble plantet i hver prøve og etter to uker viste prøvene opptil 21 røtter med en gjennomsnittlig dybde på 10 mm. Etter fire uker viste prøvene opptil 50 røtter med en gjennomsnittlig dybde på 12 mm. RVD-middelverdien var 0,2 % etter to uker og 1 % etter fire uker, og RAR nådde en gjennomsnittlig verdi på opptil 0,4 % over kolonnedybden. Porøsitetsverdiene på tvers av alle prøvene var i gjennomsnitt 64 % før plantingen, 54 % etter to uker og 37 % etter 4 ukers vekst. Den første gruppen hadde 10 % gipsinnhold uten organisk avfall, 5 % acaifrøavfall eller 5 % organisk matavfall. Den andre gruppen hadde 5 % gips med 5 % acaifrøavfall eller 5 % organisk matavfall. Den første gruppen viste varierende grad av rotutvikling. Prøven uten organisk endring viste høyest rotvekst, mens det ble observert tydelige forskjeller mellom prøvene med acai- og matavfallsendringer. Den andre gruppen hadde svært dårlig til ingen vekst. Klyngeanalyse stemte overens med inter- og intragruppevariasjonen i rotutvikling. Det ble funnet en sterk korrelasjon (R^2=0,95) mellom RD og elektrisk ledningsevne (EC) og i mindre grad (R^2=0,83) med kalsium- (Ca) konsentrasjon. Videre var RAR og RVD negativt korrelert med alkalitet med R^2-verdier på henholdsvis 0,72 og 0,64. Det ble konkludert med at digital bildeanalyse basert på µCT er en effektiv metode for å analysere røttene og porøsitet i bauksittrester og at rotvekst er signifikant assosiert med EC, Ca-konsentrasjon og alkalinitet i blandingene. Disse sammenhengene påvirkes i stor grad av utvaskingsprosedyre, vektandel av gips og type organisk avfall som brukes som tillegg.

Acknowledgment

I am thrilled to have had the opportunity to work on a project that has a tangible impact on reducing our environmental footprint and embodies the motto "Knowledge for a better world". This project served as a unique intersection of diverse fields and presented me with various challenges for personal growth. I am grateful to the Norwegian University of Science and Technology (NTNU) and the Norwegian Geotechnical Institute (NGI) for creating this remarkable opportunity.

I owe a debt of gratitude to the amazing individuals who supported me throughout this project. I would like to extend my sincere appreciation to my supervisor, Hans Peter Arp, for his invaluable guidance, trust, and flexibility in embracing new ideas for the project. I am extremely thankful to the kind professionals from NGI, Gabrielle Dublet-Adli and Vittoria Capobianco for their solid support, enriching feedbacks, and fruitful discussions. Likewise, I am deeply grateful to Hogne Phillips Stubhaug for generously sharing the raw data from his study and engaging in rich discussions with me.

I want to express a special thanks to my co-supervisor Santiago Quinteros, from NGI who introduced me to the fascinating world of image processing and CT scans. His pedagogic approach and professional attitude made our regular meetings incredibly fruitful and educational. I greatly appreciate his prompt support, even during weekends or when he was working offshore with limited internet access.

Finally, I would like to acknowledge the tremendous support of my wife Ingvild, throughout this journey. Her unwavering encouragement has been an invaluable source of strength.

Trondheim, May 2023

Table of Contents

List of figures

List of tables

List of abbreviations

Average root depth	RD
Bauxite residue	BR
Bauxite residue disposal area	BRDA
Cation exchange capacity	CEC
Dissolved organic carbon	DOC
Electrical conductivity	EC
Exchangeable sodium percentage	ESP
Filtered back projection	FBP
Ionic strength	IS
Limit of detection	LOD
Liquid to solid ratio	L/S
Magnetic resonance imaging	MRI
Micro computed tomography	μ-CT
Microwave plasma atomic emission spectrometer	MP-AES
Norwegian Geotechnical Institute	NGI
Norwegian University of Life Sciences	NMBU
Positron emission tomography	PET
Root area ratio	RAR
Root systems	RS
Root volume density	RVD
Specific surface area	SSA
Sodium adsorption ratio	SAR
Soil organic matter	SOM
Total dissolved solids	TDS
University of Oslo	UiO

1 Introduction

Aluminum (Al) and its alloys are ubiquitous in our modern lives. Owing to its high strength-to-weight ratio, good corrosion resistance, excellent thermal and electrical conductivity, and not the least, recyclability, Al has found applications in packaging, transportation, and electrical industries (Ashkenazi, 2019; Dursun & Soutis, 2014; Zhang et al., 2019). Among environmental challenges associated with the production of Al are alumina refinery tailing management, high energy demand of alumina-to-Al refining process, and accumulation of potentially toxic elements in recycled Al (Ashkenazi, 2019; Xue et al., 2016).

1.1 Red mud

Bauxite residue (BR), also known as red mud, is the sodic-alkaline byproduct of alumina (Al_2O_3) extraction from its most prominent ore, bauxite. The primary process used for the extraction is Bayer process in which the crushed bauxite ore is digested with hot caustic soda (NaOH) under high pressure. This reaction leaves behind a high pH solution in which Al oxides are readily solubilized. After several filtration and clarifying steps, the solution is calcinated for water removal resulting in the formation of a white powder that is alumina (Stubhaug, 2022). Consequently, an average of 1.354 t BR. t alumina^{-1} is produced with a global BR stockpile of 4 billion tones (Swain et al., 2022). From this amount only 2-3% is reused or further processed (Di Carlo et al., 2019). The rest of the residue is disposed in landfills which are known as bauxite residue disposal areas (BRDA). Today, dry stacking is the most common choice for BR disposal. It minimizes the land use and leakage to groundwater as compared to the lagoon-type disposal. In dry-stacking method the residual slurry, with liquid-to-solid ratio (L/S) of 3.0-4.0, is thickened to a paste with L/S of 1.0 before getting pumped to the BRDA (Xue et al., 2016). In addition to high sodicity and alkalinity, BR is highly saline and can have elevated levels of trace elements. Even after drying, the footprint of BR disposal can still reach hundreds of hectares and BRDAs potentially pose societal and environmental risks if not properly managed (Di Carlo et al., 2019; Lehoux et al., 2013).

It is a consensus that revegetation of BRDA is the most effective and efficient strategy for rehabilitation proposes not only for stabilizing the residue surface in order to decrease wind and air erosion, but also to improve landscape aesthetics (Courtney et al., 2013; De Baets et al., 2008; Di Carlo et al., 2020; Xue et al., 2016). Nevertheless, this is a challenging task as both plants and soil microorganisms struggle in such harsh conditions to support life. Along with high alkalinity, salinity, and sodicity, there are high amounts of Al, Cr, V found in BR which can be in toxic chemical forms at such high pH levels; 9.7–12.8 (Gräfe & Klauber, 2011). On the other hand, low levels of plant-available nutrition (N, P, Ca, Mg, K) and lack of soil organic matter (SOM) together with poor soil permeability contribute to limited revegetation success (Di Carlo et al., 2020; Wong & Ho, 1994). In this regard, selection of suitable plant species and pre-treatment of the residue has been a central part of the revegetation methods.

1.2 Alunorte facility

Norsk Hydro Alunorte, located in northern Brazil, is the world´s largest Al refinery (Figure 1-1). In 2021, about 11 million tons of BR were generated for the production of about 6 million tons of alumina (Stubhaug, 2022). The mining and refinery facilities are situated in the state of Pará where 93% of Brazil´s bauxite production takes place (statista, 2022).

The refinery facility and the adjacent BRDA are located in Barcarena municipality near the city of Belém and about 100 km in land from Atlantic Ocean. The average temperature of the area is 27 ℃ and the average rainfall in 3384 mm (Stubhaug, 2022).

In February 2018, following two days of extreme rainfalls, Barcarena region including Alunorte´s refinery facility suffered from flooding. The local authorities ordered certain measures such as production restriction of the facility by 50% until the investigations regarding possible harmful spills to the surroundings are investigated. More than 90 investigations and inspections took took place and confirmed that there was no leakage or overflow from Alunorte´s BRDA (Hydro, 2019).

Figure 1-1 Hydro´s Barcarena site layout. Rainwater that collects on BRDA is channeled to the edges, drained, and treated at the water treatment plant before being discharged into the Pará river. The red circles show the site of the samples used in this study. DRS and BRDA can be used interchangeably. From (Hydro, 2019).

According to the joint report by Alunorte and EcoForest, the primary environmental consequence resulting from the deposition of red mud in the BRDA Alunorte is wind-induced erosion, leading to the formation of dust clouds that disturb the local population residing in the refinery's surrounding area. Additionally, these dust clouds have a unfavorable visual impact as they cover the nearby remaining forest (Alunorte&EcoForest).

To address the issues mentioned above, Hydro aims to eliminate the need for storing new BR after 2050. In addition, there has been defined a goal for utilizing 10% of the residue by 2030 in other sectors such as construction (Hydro, 2019). Moreover, there has been several studies conducted in collaboration with Norwegian Geotechnical Institute (NGI), Norwegian University of Life Sciences (NMBU), and University of Oslo (UiO) for characterizing the BR from Barcarena as well as investigating the biogeochemical effects of various amendment regimes in the context of in situ revegetation as the main rehabilitation strategy of the Alunorte´s BRDA (Ortiz, 2021; Schneider, 2020; Stubhaug, 2022; Wik, 2020).

Ortiz (2021) investigated the effect of various amendments on BR through a batch leaching test by looking into major chemical composition changes in BR with respect to their

amendments. Models were built to assess how the amended and un-amended BR´s geochemical properties would evolve in contact with CO_2. In another study, Schneider (2020) looked into the role of density and addition of sand effect BR´s hydraulic conductivity and compaction. Wik (2020) on the other hand, characterized the BR from Alunorte with emphasis on mineralogy and chemical composition. Leaching tests were done to understand the mobility of selected elements and the role descilication products in BR.

In the more recent study, Stubhaug (2022) examined the methods for measuring cation exchange capacity (CEC) of BR. Two series of column leaching tests were done to see if addition of organic matter and gypsum in different combinations would improve the physicochemical properties of the BR, including but not limited to its pH, exchangeable Na, and aggregate stability. To test the revegetation success in the amended samples, *Lolium perenne* (ryegrass) seeds were planted and visually observed for during four weeks. In addition, dry mass of the root and shoot and length of the plant leaf were reported.

1.3 Revegetation research methodologies

Several studies exist in the literature on revegetation of the BR using various species and amendments. (Wong & Ho, 1993) investigated the effectiveness of waste gypsum as acidic amendment. Two alkaline and saline tolerant plant species were established to validate the effectiveness of gypsum and suitability of the species for revegetation. After initial leaching step of the gypsum-amended red mud, seeds were planted in the 1 cm depth of the soil and were allowed to grow for 10 weeks. The "areal portion" or shoots of the plants were nutritionally analyzed after shoot and root dry weight were registered. In another study (Courtney et al., 2009-a), samples from revegetation trials (1997-2001) from BRDA of Aughinish Alumina, Ireland were studied in terms of substrate condition, plant uptake characteristics and species diversity. Several grass- (including *Lolium perenne*) and non-grass species were planted in different sites of BRDA amended by gypsum, process sand, and spent mushroom. Dominant plant species in the sites, were used to investigate the long-term effect of gypsum application on foliar nutrient uptake, and soil samples were analysed for their chemical properties. Andersdon *et al*. (2011) used Alcoa Australia´s so called bauxite "residue fines" (particles < 150 μm) as amendments for "residue sand" (>150 μm). Pre-treated (seawater-washed or carbonated) and untreated residue fines were added to residue sands at 6 different w/w % making 18 different growth mediums. *Acacia saligna* (golden wreath wattle) was planted and grew for 13 weeks. Some physical properties and the nutrient content before and after vegetation growth were assessed. After 13 weeks, shoot biomass plus nutrient content and shoot biomass were analysed. (Jones et al., 2012) investigated the physical, chemical, and microbial effects of seawater neutralized and carbonated residue mud addition to gypsum-treated BR and its vegetation, with and without an organic waste mixture (municipal waste, a type of mulch, and poultry manure).

Majority of the studies that are done in the revegetation of BR including the selection above, share three aspects: i) BR is mixed with gypsum in combination with some sort of organic matter, ii) a leaching step prior to revegetation, iii) nutritional analysis and biomass measurements of plant tissues, after growth. Some of these studies go further and measure the length of the root and shoot as well, but there has been done to the best of my knowledge only one study, (Fourrier et al., 2021), on root development and root architectural traits of the plants grown in exposure to BR.

Fourrier *et al*. (2021) quantified the root architecture and development of two types of BR with different geographical origins, France and Guinea, and modified them with gypsum addition and leaching prior to establishing *Sinapis alba* (white mustard). The authors ran a rhizotron experiment, with normal soil on top and BR below, to assess the root development and enzymatic activity of roots in different layers within the rhizotron, after 28 days of growth. Additionally, they scanned the roots by a photo scanner, and measured root diameter, root length, number of forks, and root volume using WhinRhizo® image analysis software. It is worth to mention that although rhizotron, a soil-filled plant-growing glass box, is inherently a non-destructive root research tool, scanning of the roots need to be done by extracting them from the soil in a destructive way as it was the case in that study.

Root systems (RS) which are often referred to as the "hidden half" of the plants, have crucial role in nutrient and water uptake as well as anchorage in soil. RS continuously adapts its architecture according to spatial and temporal heterogeneity in soil´s biotic and abiotic properties. Similarly, RS modifies and stabilises soils structure through penetration, chemical exudate to rhizosphere etc. (Di Carlo et al., 2019; Jin et al., 2017).

It is important to be able to spatially and temporally study RS in each experiment to better understand its complex interaction with soil as roots for example increase branching for P acquisition in P-rich regions (Jin et al., 2017), or roots can cause different strain fields in the soil by either radial or cylindrical growth which in turn affect soil´s physical properties (Jin et al., 2013; Savioli et al., 2014). Hence, the use of non-destructive methods such as rhizotrons is beneficial. However, one of the limitations with rhizotron is that it gives us 2D views of only small portions of highly complex 3D root structures, at the soil-glass interface. We don't get to see inside the opaque soil (Hou et al., 2022).

One of the most common contemporary approaches for non-destructive sequential 3D visualization of the RS inside the soil is X-ray micro computed tomography or μCT scanning. This method provides us with high spatial resolution of 10-50 μm while many roots diameters are in the range 100-500 μm (Hou et al., 2022). Imaging with this technique can be done multiple times giving us a timeline of the root development while not disturbing the natural process of growth. The 3D images can further be analysed using advanced digital image analysis techniques for quantification of various root descriptors.

In BR literature, to the best of my knowledge, there is only one study, (Zhu et al., 2016), in which X-ray μCT technology has been utilized to show the change in porosity, specific surface area (SSA) and some other physical traits with aging of BR. No other study has been done on evaluation of RS inside revegetated BR using μCT method.

1.4 Objectives of this study

The present study builds up on Stubhaug (2022)´s work on evaluating the fate and effect of revegetation attempts in the amended bauxite residues from Alunorte in Brazil, which is line with United Nations sustainable development goal number 15, 'life on land', as it is a step towards restoration and promotion of sustainable use of terrestrial ecosystems. The revegetation success of bauxite residue disposal areas has direct environmental and societal impacts both regionally and globally, hence the importance of this research.

The main aim of the current study is to determine which amendment provided best chemical and physical conditions for the roots to grow inside the residue. To assess the revegetation success of amended bauxite residue, the following steps were taken:

1) Evaluation of root development in the revegetated amendment mixtures by analyzing their μCTs to quantify the following roots features:
   a) Number of roots and their depths
   b) Average root depth
   c) Root volume density
   d) Root area ratio with respect to depth
2) Assessment of the porosity change in the mixtures with respect to depth, during the ryegrass growth by analyzing their μCTs.
3) Latent variable analysis of the chemical data obtained in (Stubhaug, 2022) to understand the chemical phenomena that supported or suppressed root growth.

2 Theory

2.1 Bauxite residue

To better understand the nature of BR and the prospects of revegetation, it is beneficial to briefly summarize the Bayer process which leads to the generation of BR. Moreover, some of the relevant physical and chemical properties of BR are discussed below, which can play a role in reactivity of solid particles and soil structure. For instance, bulk density and porosity are related to hydraulic conductivity which is directly related to water and nutrition availability to the plant roots whereas pH affects the toxicity levels.

2.1.1 Bayer process

Bayer process is a dissolution process under high pressure and temperature for extracting gibbsite ($Al(OH)_3$) and/or boehmite (γ-AlOOH) from bauxite ore by dissolving those constituents in caustic soda (NaOH) (Gräfe et al., 2009). The process is comprised of 5 physical and chemical major steps to obtain alumina as a white powder; grinding, digestion, clarification, precipitation, and calcination as shown in Figure 2-1 (Jones & Haynes, 2011). Here, we will focus on the first three steps as they are those which lead to BR generation.

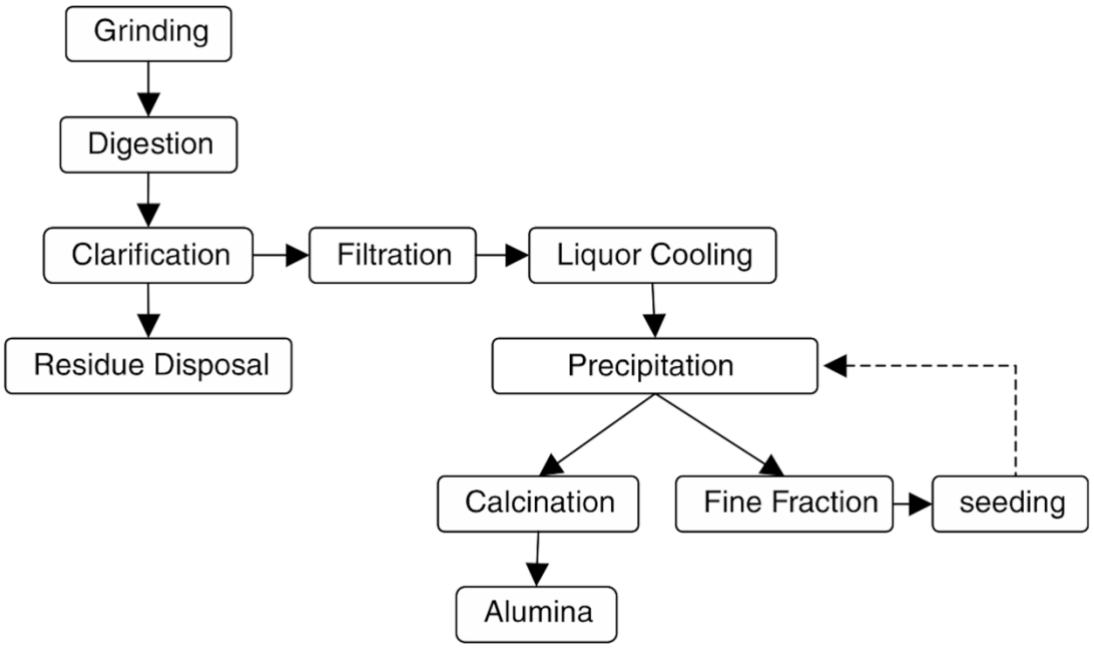

Figure 2-1. Schematic diagram of Bayer process from (Jones & Haynes, 2011).

In the preliminary step, the bauxite ore is washed to remove unwanted materials like residual clays which may interfere with the efficiency of the process. Next, the washed ore is crushed and ground, which increases the martials SSA hence improves the extractability of its components. The grinded ore is then treated with hot caustic soda (NaOH) and wet ground to form a slurry. The slurry is stored in tanks before being transferred to the digestion unit. This allows time for removing silica from the liquor (predesilication phase) (Jones & Haynes, 2011).

Once the slurry is transferred to the digestion unit, it is mixed with additional caustic soda. Then the resulting slurry is steam-heated in either autoclaves or tabular reactors where the digestion process takes place. During the digestion process, hydrated alumina is separated from other insoluble oxides by reacting with sodium hydroxide:

$$Al_2O_3\,.\,xH_2O + NaOH \longrightarrow 2NaAlO_2 + (x + 1H_2O) \qquad [1]$$

It is the composition of the bauxite that defines the effectiveness of the digestion step. Different Al-bearing minerals have different solubilities. It is the strength of the hydrogen bonds in those minerals that determines their solubility. For instance, gibbsitic bauxite has the weakest hydrogen bonding thus requires temperatures up to 150℃ while boehmitic bauxite requires 200-250℃ and pressure 3.45 MPa to be completely digested. Likewise, concentration of NaOH is adjusted based on the mineral profiles of the bauxite; 3-7 M NaOH. Gibbsite-rich bauxite is more operationally favored as its extraction happen quickly in a matter of few minutes thus less energy input is needed (Jones & Haynes, 2011).

Caustic degradation of humic substance in Bayer solution results in formation of sodium carbonate (Na_2CO_3; 18-51%), and sodium oxalate ($Na_2C_2O_4$; 2-16%), during the digestion step. The crystallization of sodium oxalate crystallization poses one of the main limitations on the effectivity of the process. The crystallization chemical rection is shown below:

$$2Na^+_{(aq)} + \ C_2O^{2-}_{4\,(aq)} \leftrightarrow Na_2C_2O_{4\,(s)} \qquad [2]$$

Gibbsite can be nucleated by sodium oxalate crystals owing to their fine needle-shaped form. The nucleation of gibbsite hinders its agglomeration which results in fine gibbsite particles unsuitable for subsequent calcination in the downstream process (Jones & Haynes, 2011).

The NaOH solution now contains supersaturated sodium aluminate $NaAl(OH)_4$, known as green or pregnant liquor) and BR solids. In the clarification phase these two fractions are separated in a stepwise manner. First, the coarser parts aka residue sand of both fractions is removed by gravity, washed to remove NaOH, and eventually pumped to disposal operation units. Next, the finer particles also known as residue mud is separated by flocculation, aided by starch and synthetic flocculants, in thickener vessels. In the subsequent washing step, an underflow of 50% solid slurry is created through a countercurrent washing train.

The overflow stream goes through a causticization process to maximize the soda recovery. in this process, the stream is heated and contacted with lime slurry. Hydrated lime reacts with sodium carbonate and precipitate calcium carbonate:

$$CaO\ or\ Ca(OH)_2 + \ Na_2CO_3 \leftrightarrow CaCO_3 + 2NaOH \qquad [3]$$

At the end of the clarification process, the last traces of solid material filtered out prior to BR disposal (Wik, 2020). The BR still remains strongly alkaline even after repeated washing since big portion of the alkalinity comes from slowly dissolving solid phases (Gräfe et al., 2009).

2.1.2 Physical and chemical characteristics of BR

2.1.2.1 Physical properties

The average particle size of BR ranges from 2 to 100 μm while the typical range is 100 nm to 200 μm (Gräfe et al., 2009). The particle size distribution is a function of the separation

of sand-size particles after alumina extraction whereas it is the disposal method (lagooned vs. dry-stacking) which determines the texture of the residue. The texture defines how different particle sizes are separated in the BRDA (Gräfe & Klauber, 2011).

The bulk density of unamended BR has been reported to be 2.5 ± 0.7 g·cm^{-3} on average, which is considered as high. Bulk densities above 1.5 g cm^{-3} impede penetration of roots and thus the plant establishment (Gräfe et al., 2009). Amendment of BR with gypsum to a lesser extent and with organic material (with low bulk density) to a greater extent can dilute the denser mineral fraction of BR and consequently decrease the bulk density (Di Carlo et al., 2019). Bulk density is influenced by physical conditions such as the amount of organic matter, soil structure, and porosity (Xue et al., 2016).

Porosity is defined as the ratio of the total volume of pores or voids to the total volume of the sample expressed in percentage (Gräfe & Klauber, 2011), and is one of the indicators that has been widely used for evaluation of physical quality of mine residues (Zhu et al., 2016). The porosity of unamended BR, compost-, and compost+gypsum-amended BR has been reported to be 59, 65.9, and 64.3%, respectively (Courtney et al., 2013).

The hydraulic conductivity of unamended BR is reportedly 0.002 cm·min^{-1} which is very low (Gräfe et al., 2009). This is due to the consolidation of fine BR particles which form a solid mass with very few large-enough pores for passage of water, nutrition, and air. The outcome is very low infiltration rates and plants can seldomly survive under such conditions (Xue et al., 2016).

2.1.2.2 Chemical properties

The master variable, pH

Most chemical reaction are partially a function of pH as it can either drive a reaction backward or forward. The high pH of BR is caused by NaOH and lime (CaO) addition in the Bayer process which forms multiple alkaline solids such as hydrate garnet and sodalite. The concentration of remainder of added NaOH and the unreacted sodium carbonate in the solution, bring about an average solution pH of 11.3±1.0. We should note here that this value corresponds to the aged BR which has been partly neutralized by atmospheric CO_2. High soil pH adversely affects the root respiration and growth, and root-pressure-driven solute export to xylem (Gräfe & Klauber, 2011; Gräfe et al., 2009; Xue et al., 2016).

It is only when alkaline solids have dissolved and the associated reaction products are removed, that pH can be reduced (Xue et al., 2016). This is complicated to achieve because for instance Na_2CO_3 (sodium carbonate), among other alkaline-sodic components, exists in quasi-equilibrium with the BR solution (Gräfe & Klauber, 2011).

pH determines the solubility state at which compounds are present in any solution including the BR solution. For example, $Al(OH)_3$ is readily dissolved at pH 4.0 and 13.0 while it is quite stable at pH 7.5 as shown in Figure 2-2 (Gräfe et al., 2009; Johan et al., 2021). In BR solution, the soluble aluminate ion, $Al(OH)_4^-$ together with $HCO3^-$, CO_3^{2-}, and OH^- are the main alkaline ions that buffer the solution. Aluminate ion and elevated levels of soluble Fe, which is the case in BR, are negatively correlated with essential macronutrients for plants such as P, N, K, Mg, and Ca while soluble Al and Fe are positively correlated with each other (Xue et al., 2016).

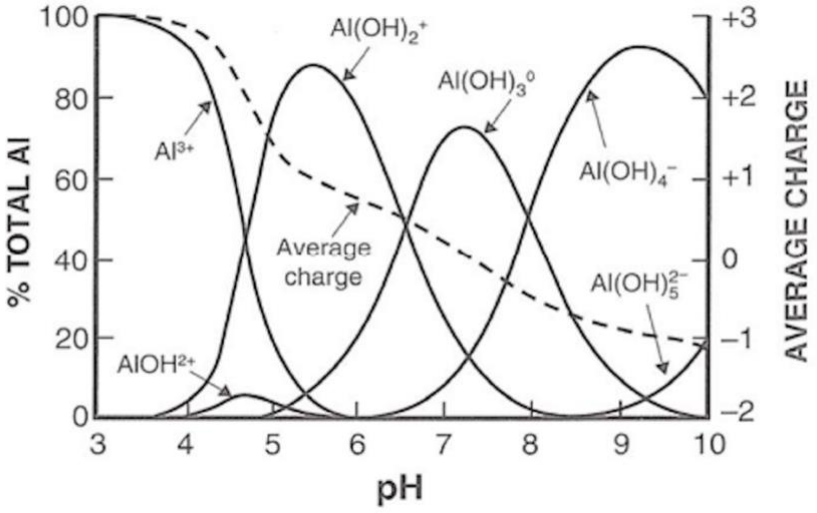

Figure 2-2. Distribution of soluble aluminum species with respect to pH. From (Johan et al., 2021).

Sodicity

The insistent abundance of remnant sodium (Na^+) in BR, as one of the major barriers for revegetation, goes hand in hand with high pH as it encourages the hydrolysis of Na_2CO_3. High amount of sodium in soil is associated with dispersion. Clay dispersion happens when the electrolyte (e.g., Ca, Mg, K) concentration in soil environment is below flocculation value of the clay. Since CO_3^{2-} is present and pH is high, Ca^{2+} and Mg^{2+} precipitate and therefore their concentration in the solution is low (Sparks, 2003). The Na^+ concentration in BR solution had been reported to be exceeding Ca^{2+} and Mg^{2+} by 2-4 orders of magnitude (Gräfe et al., 2009).

Poor flocculation results in poor aggregation and thus poor hydraulic conductivity. Cementation and dust formation are other consequences of combined high sodium ion and pH levels. Moreover, high sodium ion content increases the solutions electrical conductivity to intolerable levels for plants and deprives them from water uptake (Gräfe et al., 2009). In addition, excess Na uptake interferes with cytoplasmic enzymatic reactions and reduced uptake of other elements, such as Ca, Mg, and K. Ca deficiency in turn influence the cell membrane leading to N, Mn, Zn, and Cu deficiencies (Di Carlo et al., 2019; Xue et al., 2016).

Saline cations have different and temporally distinct migration behavior in BR environment thus different vertical distribution profiles. It has been indicated in (Kong et al., 2018) that Na^+ has a weaker colloidal adsorption as compared to Ca^{2+} and K^+, as shown in Figure 2-3, being affected by ionic radius, charge, and concentration. The authors argued that sodium ion has stronger intermolecular force interaction with hydron rather than with BR´s colloidal particles. The vertical distribution of ions plays an important role in RS architecture because roots always aim to optimize the plant´s uptake of water and nutrition and avoid (sodic-) stressed regions in soil.

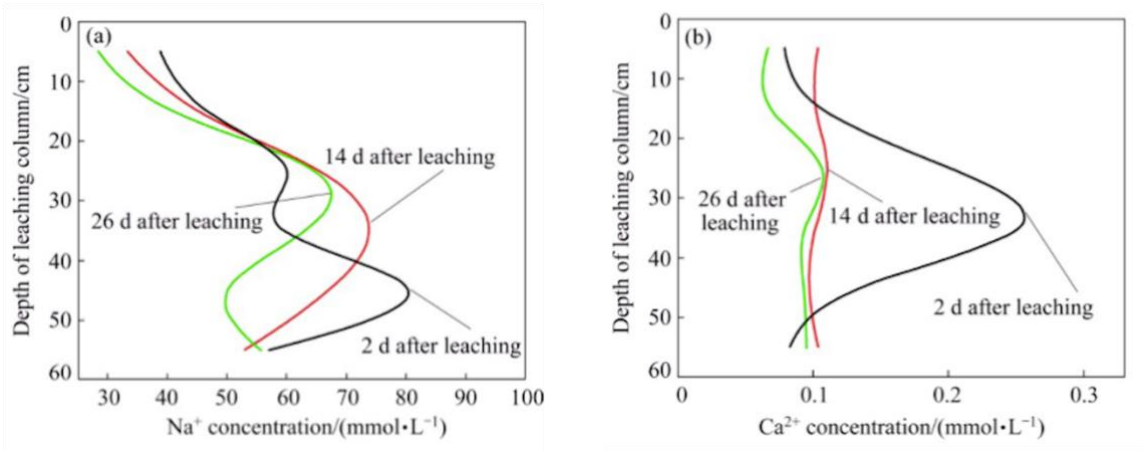

Figure 2-3. Vertical distribution of sodium and calcium ions in BR for 26 days of leaching. Note the difference in concentration of the two ions as maximum calcium ion concentration is approx. 2 orders of magnitude less than minimum sodium ion concentration. Extracted from (Kong et al., 2018).

There are different parameters that are used to measure sodicity such as exchangeable sodium percentage (ESP) and sodium adsorption ratio (SAR). ESP is the concentration of exchangeable Na^+ as per total exchangeable cation (Ca^{2+} + K^+ + Na^++ Mg^{2+}). A soil is recognized as sodic if ESP>15%. In unamended BR the typical ESP value is 60-90% rendering it as highly sodic (Di Carlo et al., 2019). ESP value estimates the composition of the cation exchange site on BR surface based on composition of Na, Mg, and Ca (Gräfe & Klauber, 2011).

SAR on the other hand, like pH, is a solution parameter while being dependent on the nature of the solid that the solution is contacted with (Gräfe & Klauber, 2011). As it can be seen in the equation [4], SAR treats Ca^{2+} and Mg^{2+} as if they are the same atoms even though they have different ionic radius. This is based on empirical observations that valance number is more significant in predicting ion exchange phenomena as opposed to ionic radius (Sparks, 2003).

$$SAR = \frac{[Na^+]}{\sqrt{[Ca^{2+} + Mg^{2+}]}} \qquad [4]$$

Where brackets show the total concentrations of the ions in mmol·liter^{-1}.

Although ESP is used to distinct sodic and non-sodic soil, it often lacks accuracy due to the problems with measurements of CEC and exchangeable Na^+ (Sparks, 2003) as their values can be overestimated (Stubhaug, 2022). Therefore, it is easier to use SAR as the criteria for sodic hazard evaluation such that value greater than 13 render the soil as unsuitable for plant growth. pH, ESP and SAR are all interrelated in the context of NaOH and $Ca(OH)_2$ inputs from Bayer process and the mineralogy of BR. To that end, ESP and SAR can be related by the following equation (Gräfe & Klauber, 2011):

$$ESP = \frac{1.5 * SAR}{1 + 0.015 * SAR} \qquad [5]$$

Salinity

High concentration of soluble salts, or salinity, is another major problem inhibiting plant growth. There are different indices to represent salinity of which total dissolved solids (TDS) and electrical conductivity (EC) can be mentioned. EC is the preferred index as its

measurements are reliable, quick, and inexpensive. In amended BR, EC varies between 0.3 to 60 $mS{\cdot}cm^{-1}$. It is based on the concept that electrical current in a salt solution under a standard condition, increases with increasing salt concentration. EC is closely related to concentration of anion and cations thus to the ionic strength (IS). IS is approximately 0.0127 times the EC as it has been shown in Figure 2-4 (Gräfe et al., 2009; Sparks, 2003).

It is important to note here that this proportionality holds only for the treated BR whose alkalinity levels has been reduced. In the highly alkaline untreated BR, the ionic species are not completely dissociated therefore the assumption of equivalent conductance at infinite dilution is meaningless (Gräfe & Klauber, 2011).

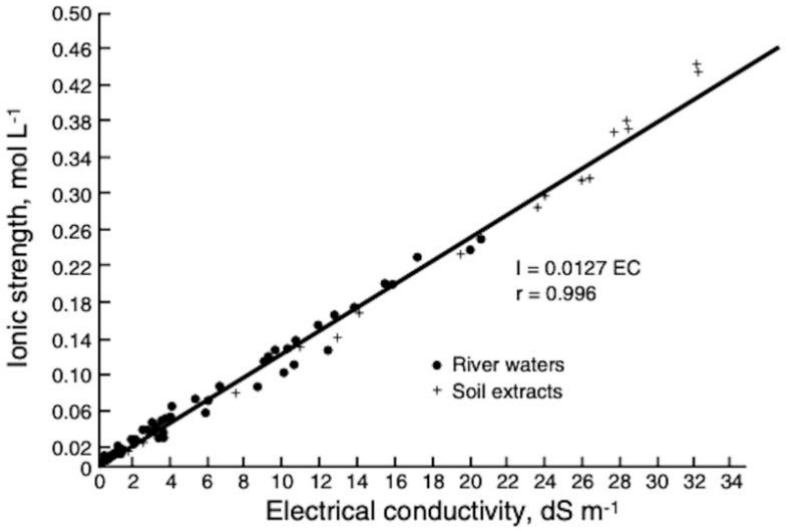

Figure 2-4. Relationship between electrical conductivity and ionic strength of natural aqueous solutions. From Sparks (2003).

The IS is an important parameter as it i) indicates the osmotic potential of the solution as it becomes increasingly negative as ion concentration increases, and ii) determines the double-layer thickness of charged BR clay particles (Gräfe & Klauber, 2011). The reduced osmotic potential impedes water uptake by roots. At the same time, high IS value is related to decrease in the double layer thickness leading to dispersion.

As we have seen so far, the combined effect of high pH, sodicity, and salinity is multifacetedly negative for plant growth and bears physical, chemical, and biological stress. Therefore, before any revegetation attempt, rehabilitation of BR is not an advantage but a necessity.

2.1.3 Amendment of BR

Combination of organic matter and gypsum is the most effective treatment to bring down the pH as it has been shown in both laboratory and field studies. In addition to their acidifying properties, these amendments can reduce exchangeable Na and extractable Al while increasing exchangeable Ca. This combination has been reported to be decreasing soluble As and V levels which are potentially toxic to the plants (Di Carlo et al., 2019).

Gypsum ($CaSO_4$) earns its efficacy in lowering the pH by realizing Ca^{2+} and consequently precipitating excess $(OH)^-$, $CO3^{2-}$,and $Al(OH)^{4-}$ as $Ca(OH)_2$, $CaCO_3$, hydrocalumite, and TCA (Gräfe et al., 2009). Gypsum is also effective in lowering sodicity by replacing Na^+ with Ca^{2+} on cation exchange sites of negatively charged particles as the divalent Ca^{2+} is

more strongly held to those sites. With leaching involved, the Na will be leached down the soil column. Thus, upon Ca addition by gypsum there is sharp fall in ESP followed by a slower decrease as Na leaches out of the profile (Di Carlo et al., 2019; Kong et al., 2018). Also, the flocculating effect of calcium may replace the dispersive effect of sodium ion which in turn would increase micro-aggregate stability and hydraulic conductivity in the BR (Xue et al., 2016).

Organic matter reduces pH by means of its organic acids and CO_2 that is produced upon it´s respiration. These materials may additionally supply plant with nutrients through mineralization, mitigate metal ions by forming stable complexes with them, reduce soil compaction, provide energy sources to soil microorganisms, stabilize soil structure, and stimulate soil aggregation (Xue et al., 2016).

2.2 Root-soil interaction

The primary role of the RS is to acquire soil nutrients and water, and to provide anchorage for the plants. The relationship between roots and soil though is complicated and can be labeled as bidirectional since soil properties affect root architecture-growth and roots in turn modify the soil environment as they penetrate.

Nutrient availability varies both spatially and temporally in the complex soil environment which generates changing arrangement of soil patches. This happens naturally in soils and therefore plants have adapted to this by changing their architectural traits in order to optimize uptake of nutrient and water. For instance, roots increase their branching in P- or nitrate-rich patches of the soil (Jin et al., 2017). The physical condition of the soil too has a say in accommodating RS as roots elongate within an existing crack/pore or they negotiate a new one (Jin et al., 2013).

Roots, on the other hand, can modify soils biological, chemical, and physical properties through various paths. 20-40% of the photosynthetically fixed C by the plants is devoted to root exudates which are sugars, organic acids, and amino acids. Plants secrets these chemicals to encourage the beneficial microorganisms, promote nutrient acquisition, and even enabling self- and non-self-roots recognition. The concentration change of exudates at the tip of the roots is sensed by the plants and can be translated into architectural changes such as lateral root formation (Canarini et al., 2019).

Upon penetration through small pores, roots can deform soil structure and make new channels (Jin et al., 2013). Based on X-ray CT of the root tip geometry and numerical simulations (Savioli et al., 2014) observed that radial expansion of roots induces compressive stress everywhere in the soil with a maximum stress release at the tip which dilates the soil around the root tip facilitating axial expansion. Moreover, water uptake by roots leads into increase in soil strength through induced soil suction. Since RS´s water extraction is heterogenous throughout soil, tensile stresses emerge in soil system which give rise to production of dense aggregates (Jin et al., 2017).

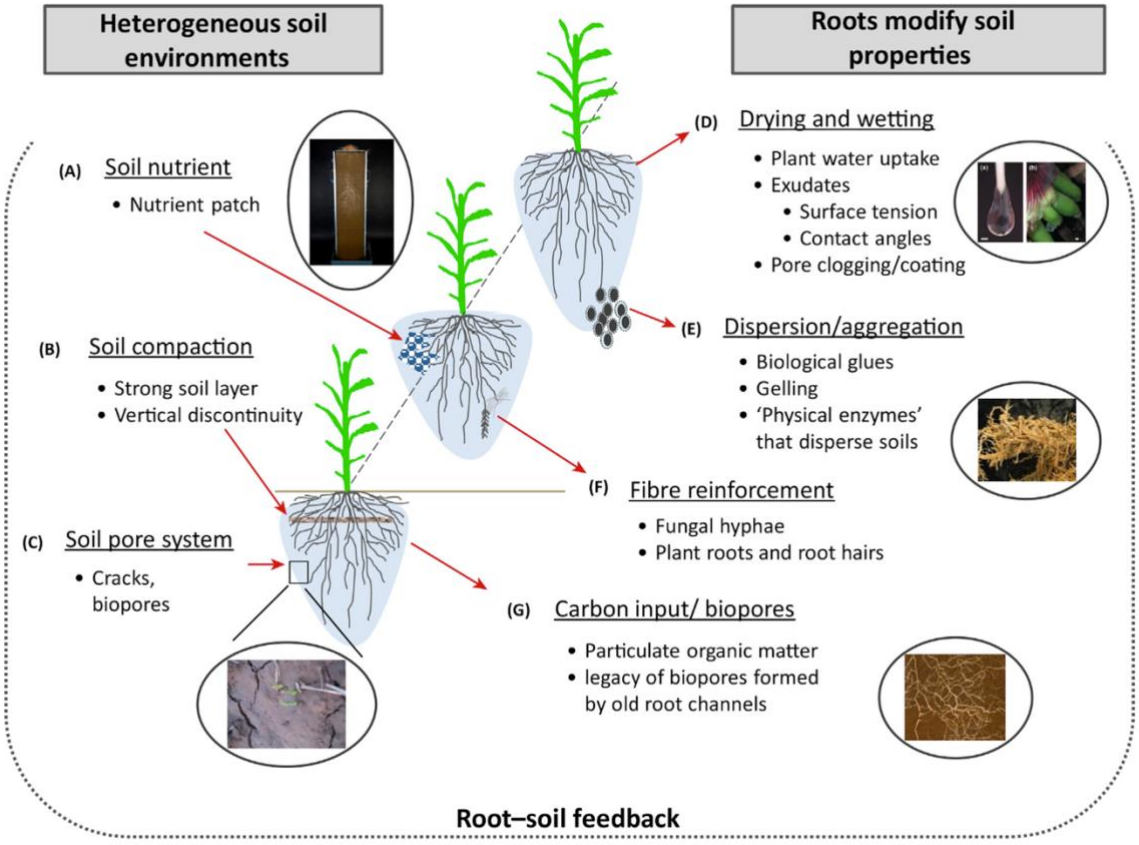

Figure 2-5. Root-soil interaction based on heterogenous soil condition. (A) Plants grow faster and branch out more when they encounter nutrient-rich soil. B) Soil compaction and structure affect root growth, especially when there are sudden density changes between layers. C) Soil pore system is diverse due to nutrient and water migration as well as soil management, and plant roots can change soil structure for the sake of their own growth. D) Roots absorb water from the soil in a spatially heterogenous way, which leads to the creation of small soil aggregates. E) Mucilage and water released from roots can increase soil water content, and root cap cells can bind soil together and form aggregates. F) Roots interact with microbes to improve soil stability, and root hairs help penetration in the soil. G) Plant roots can improve soil structure over time by contributing to organic matter and pore formation. Note that not all the aspects in the figure are relevant to BR (e.g., biopores) as these are for naturally occurring soils while BR is a product of man-made process with very altered properties. From (Jin et al., 2017).

Soil compaction, a vertical discontinuity in soil´s density, is a complicated phenomenon in soil that is closely interrelated with root growth. As mentioned above, water uptake by roots can lead into compaction by forming dense aggregates. Furthermore, soil pore space, nutrient availability and mechanical resistance of soil are all modified by soil compaction. This will in turn limit the root growth in dense areas and gives the opportunity to proliferate in looser zones in soil (Jin et al., 2017).

The effect of roots in protecting soil from erosion cannot be underestimated. Roots affect soil´s infiltration rates, moisture content, aggregate stability, and organic matter content, all which control erosion rates of the soil to certain extents. Plant roots can increase soil´s shear strength indirectly by water removal and directly by mechanical reinforcement. One important mechanical characteristic of roots is their high tensile strength while soil is known for its compressive strength and tensile weakness (De Baets et al., 2008). Foresta *et al.* (2020) found a positive correlation between the integrated friction angle, a shear strength parameter, with the root volume density (RVD) of the perennial *graminae*

grasses. The mechanical effect of roots in soil is analogous to that of steel mesh (high tensile strength) in the concrete slab (high compressive strength), an engineering solution for carrying tons of loads.

Interspecies differences in tensile strength of roots are less substantial to soil stability than interspecies differences in distribution of roots. Root area ratio (RAR) also known as root biomass concentration as a function of depth in soil is a measure developed to estimate contribution of roots to soil strength. RAR is defined as the root-occupied fraction of soil´s cross-sectional area per unit area (De Baets et al., 2008).

2.3 Studying roots with X-ray microcomputed tomography

Computed tomography, a reinvention of X-ray imaging, was first developed for imaging the skull by the English engineer Godfrey Hounsfield in 1972 while he was working at EMI (Hounsfield, 1973). EMI was the recording company for The Beatles whose huge profit partook in funding the development of CT (Saltzman, 2009). Prior to that in the early 1960s, Allan Cormack was working independently on the underlying mathematics behind reconstruction of three-dimensional images (Cormack, 1963). The main idea was to take many X-rays images from many different angles to reconstruct a three-dimensional image of the body. These three-dimensional images could then be presented as two-dimensional cross-sections which exposed the relationships between the body tissues (Saltzman, 2009).

Today CT as a non-invasive, non-destructive technique is used to examine the internal structure of many objects since it is based on the principle of attenuation of X-ray beam that is focused on the object. Unlike the conventional two-dimensional X-ray images (density shadow radiographs) in which the depth information is lost, in CTs the beam transmission information is obtained from radiographic images from multiple angles and are used to reconstruct a three-dimensional image. The ability of this method in providing detailed information about phase interfaces in a non-destructive way, makes it a great tool for geometrically characterizing the porous medium such as soil. Allowing for repeated measurements without a requirement for any pre-treatment of the samples, are among the reasons that this technique has found applications in medicine, agronomy, geology and so forth (Pires et al., 2010; Wildenschild et al., 2002).

2.3.1 Fundamentals, cons, and pros of X-ray CT

As the X-ray beam penetrates through a sample material, it loses some of its intensity. This reduction in intensity which is a function of the material's thickness and density is referred to as attenuation. The beam that passes through the sample is then projected to a detector which create a 2D-image based on the intensity changes due to attenuation. These images reveal an average composition of the sample´s thickness at the point of X-ray incident because of the difference in attenuations of different components. The images are utilized to create a complete sample reconstruction (known as CT) to obtain virtual cross-sections throughout the thickness of the sample (Hou et al., 2022).

While the sample is gradually rotated within the incident beam, each virtual cross-sectional slice is acquired through the sample by collecting several individual images. In medical CT-scanners both the detector and the beam source rotate around the subject. In industrial scanners it is the sample which rotates around a fixed detector and beam source as shown

in Figure 2-6. The multiple images (projections) from this step are used to construct a single cross-sectional image that show a virtual 2D cross section (slice) through the 3D object. This process is called image reconstruction which uses different mathematical approaches with the most commonly used being filtered back projection (FBP) (Hou et al., 2022).

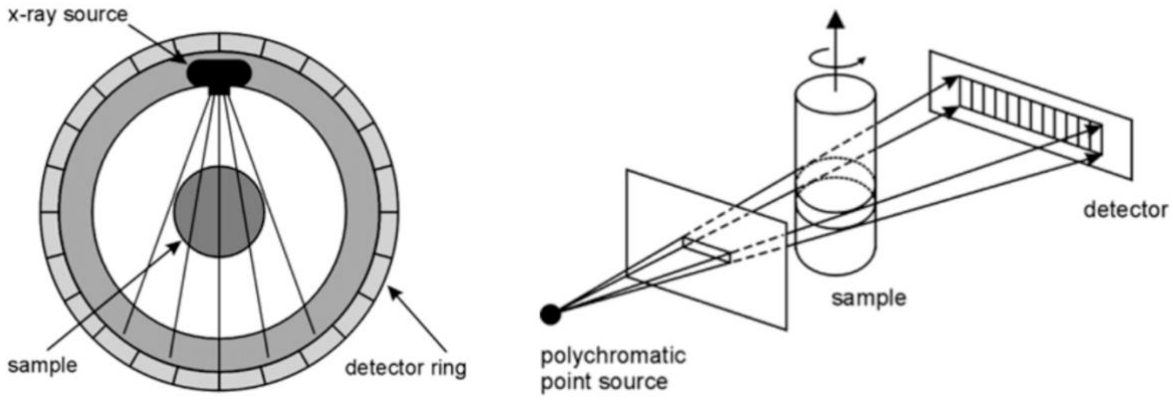

(a) (b)

Figure 2-6. An illustration of (a) medical and (b) industrial CT scanners. Extracted from (Wildenschild et al., 2002)

Commercial industrial and medical scanners both use polychromatic beam as X-ray source. Polychromatic beam is a product of a broad spectrum of frequencies from 10^{16} to 10^{21} Hz, corresponding to 10^{-8} to 10^{-11} cm wavelengths, and photon energies from 200 to 100.000 eV. This spectrum of electromagnetic waves is combined result of the processes that take place in an evacuated glass bulb containing two electrodes. As a high voltage is applied between the two electrodes, the cathode rays (accelerated electrons) generate electromagnetic radiation (X-rays) as they strike the anode (Wildenschild et al., 2002).

An X-ray beam is described by its spectral energy distribution, and photon flux density. As a beam passes through an object, the material itself becomes a secondary source of electrons and X-rays. Due to these secondary processes, the primary beam is partially scattered or reabsorbed out of the beam. If the X-ray radiation is monochromatic with an incident intensity of I_0, the attenuated intensity of the beam, I, after passing through a sample with thickness D(L) is described by Lambert-Beer´s law (Wildenschild et al., 2002):

$$I = I_0 \exp(-\mu D) \qquad [6]$$

Whereas μ is the linear attenuation coefficient of sample with unit (L^{-1}) and depends on the energy of the radiation, electron density of the material and the bulk density of the material. The attenuation of polychromatic X-rays are assumed to be governed by equation [6] despite the fact that they are subject to the preferential absorption of the photons with lower energies by the matter (Wildenschild et al., 2002).

The preferential absorption of lower energy photons in polychromatic beams by sample material, results in a lower average beam energy at object´s boundaries and higher average beam energy inside the object. This means higher attenuation coefficient on the interface and lower attenuation coefficient within the otherwise homogenous scanned object. Attenuation coefficient thus affects the intensity sensed by the detector. This phenomenon is called ´beam hardening´ and results in artifacts in CT images. Figure 2-7

shows some simulated artifacts that are caused by beam hardening. This can be an important limitation in inspection of root-soil systems. The longer the beam path inside the object the more pronounced the beam hardening. However, beam hardening artifacts can be reduced by i) reducing sample size, ii) pre-hardening the beam with a filter, iii) correction while reconstructing the image (Boas & Fleischmann, 2012; Hou et al., 2022; Wildenschild et al., 2002).

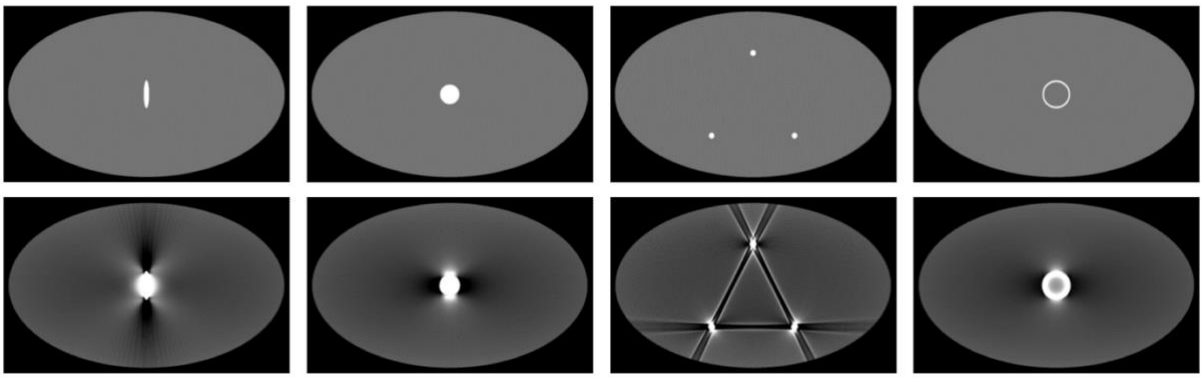

Figure 2-7. CT scans showing the beam hardening artifacts in the bottom row and the scans without artifacts in the upper row. From (Boas & Fleischmann, 2012).

Besides beam hardening as an error source for CT analysis, spatial resolution and contrast sensitivity are other limitations that are related to the type and size of X-ray source and detector as well as the sample material in question and its relative position to the source and detector. Therefore, it is important to select the appropriate X-ray source for the given sample. The rays should be energetic enough to penetrate the sample that can eventually render a well-detailed image. On the contrary, if the source is too powerful, the relative attenuation will be decreased and the object will appear transparent with little to no phase contrast (Wildenschild et al., 2002).

In studying root-soil systems, a key limitation is the trade-off between the spatial resolution and the soil column size. A column with a large diameter requires a higher photon energy for effective penetration but a side-effect of this high energy is a lower contrast which hinders root identification inside the soil. The flipside to that coin is that lower diameter will lead to alteration of RS architecture as the roots begin to grow in circling patterns rather than outward. In other words, plants become ´pot bound´. Another limitation of CT for RS studies is that the contrast resolution of X-ray CT is not necessarily as high as for example magnetic resonance imaging (MRI) and positron emission tomography (PET) techniques. This is a matter of concern as the X-ray attenuation difference between roots, air pores, water, and soil organic matter is generally small (Hou et al., 2022).

Despite of the (manageable) limitations mentioned above, CT has certain advantages over other *in situ* techniques. For instance, in MRI, only soils free of magnetic particles can be scanned. As most soils are quite high in Fe concentration, in MRI applications for root-soil, either artificial growth medium for roots should be used, or the soil should be rigorously sieved to remove magnetic components. In addition, the voxel (smallest volumetric unit of a 3D CT image) size of current CT systems is in the range of 10-50 μm while MRI systems have spatial resolution of 500-2000 μm. This renders CT more suitable for root-soil studies as many roots have diameter in the range 100-500 μm. Moreover, X-ray CT systems are often faster in image acquisition (Hou et al., 2022).

2.3.2 Use of X-ray CT in root-soil systems

The first use of X-ray CT in soil science was done by (Petrovic et al., 1982) to determine soil bulk density, soon after the development of CT in the medical field. They showed a linear relationship between the X-ray attenuation and soil bulk density. Subsequently, in (Hainsworth & Aylmore, 1983), CT was employed for repetitively measuring spatial distribution of water content of the soil and a single plant root water uptake, in a non-destructive manner. In the following two decades there was an increasing interest for CT in soil research owing to technological advancements in the scanners such as improved spatial resolution as well as image processing advancements such as computing capacities (Taina et al., 2008).

Helliwell *et al*. (2017) used X-ray CT to study the changes in rhizosphere physical structure at early stages of root development of tomato (*Solanum lycopersicum*). The experiment involved four replicate samples from both loamy sand and clay loam soil types. They observed a high variation within the treatment due to variable lateral root proliferation and that porosity increases locally around the lateral roots. Moreover, the zone immediately at the root surface showed higher porosity while bulk soil (farther away from root) had lower porosity (Figure 2-8). They concluded that the porosity of rhizosphere in the vicinity of roots increased initially but thereafter, it decreased in loamy sand and increased in the clay loam.

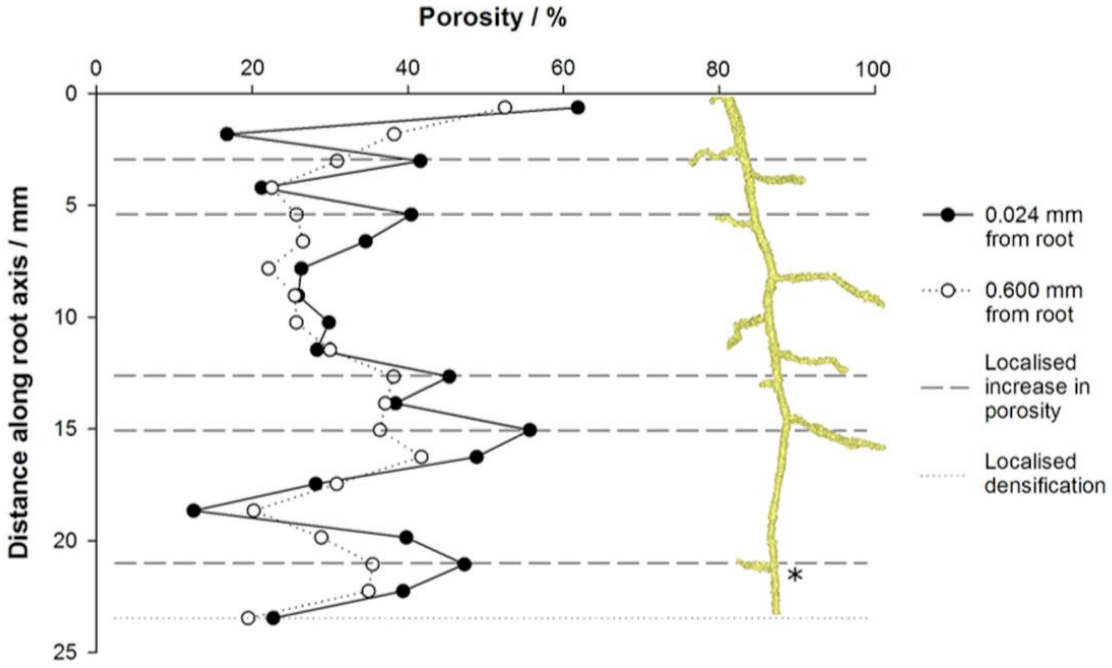

Figure 2-8. The impact of roots on soil porosity, shown at two different distances from the root surface (0.024 mm and 0.6 mm) after 8 days. The area where roots grow is represented by a star symbol. The figure displays zones of increased porosity (pores) and decreased porosity (densification), which differ based on the type of root. From (Helliwell et al., 2017).

In a study by Fang et al. (2019), X-ray CT was used to investigate the influence of puddling intensity of rice paddies the structure of the soil and the consequent effect on rice seedling roots. Paddling is done to create a soft soil bed to ease up the transplantation of rice seedlings, among others. Root 3D architecture traits and soil pore structures were determined using image analysis techniques. Roots 2D traits were determined using the

WinRhizo method. They concluded that primary roots are not influenced by paddling while lateral root growth are limited by that process.

In a more recent study (Kemp et al., 2022), the growth of a single *Achillea millefolium* seed in two different layered-soils in columns with 32 mm inner diameters in 15 days was assessed. Their aim was to assess the interplay between soil structure and root growth. Columns of different samples contained four homogenous layers (clay, silt, sand, gravel) with two different vertical arrangements of the layers. They developed a machine learning algorithm that was able to segment the root from soil in CT scans and quantify the root volume ratio and void ratio of the soil. In most cases, the void ratio increased because of root growth although they also observed root expansion induced compaction in the sand layer in the sample with gravel on top and sand as the second top layer (Figure 2-9). They concluded that the root-induced changes in rhizosphere is dependent on the soil structure.

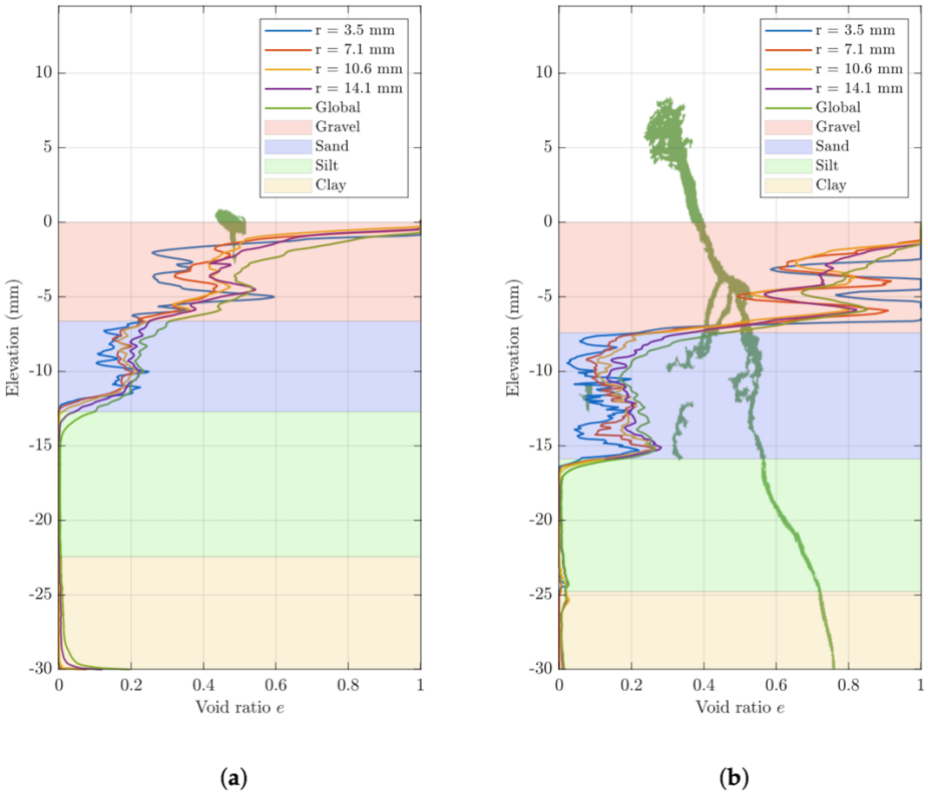

Figure 2-9. Changes in void ratio with elevation for one of the samples with gravel on top and sand as the second top layer on Day 1 (a) and Day 15 (b). The radius of the region of interest is shown as r. Figure extracted from (Kemp et al., 2022)

3 Materials and methods

Below some the material and method from (Stubhaug, 2022) are summarized in section 3.1 as they are necessary information for understanding the background of the samples. Sections 3.2-4 are the material and method that were utilized for the current study.

3.1 Columns leaching tests

In the previous work, column leaching tests were performed to analyze the leachate of different columns with different amendments. The residue that was used in that study were fresh (unaged) and taken from before the conveyor belt transferred them to the BRDA after having passed through the filter press (Stubhaug, 2022)

3.1.1 Column preparation

Five triplicates of X-ray transparent plastic cylinders were constructed at NGI for the leaching test and subsequent vegetation, with the inner diameter of 5 cm and 25 cm height. Each cylinder had rubber cap at the bottom with a drainage valve to let the leachate through the connected tubes. Above the cap, there was a 1 cm high sand layer to prevent the fine-textured BR from being washed away while letting the water through. This layer itself was supported by a filter paper underneath. The BR in each of the 5 groups received a different amendment mixture. Each mixture contained different weight proportion of BR, gypsum, acai, and organic food waste as it is shown in Table 3-1 (Stubhaug, 2022).

Table 3-1. The composition of different amendment mixtures.

Treatment	Gypsum (G) (%)	Acai waste (A) (%)	Organic waste (O) (%)	Bauxite residue (BR) (%)
BR90-G10	10	-	-	90
BR90-G5-O5	5	-	5	90
BR90-G5-A5	5	5	-	90
BR85-G10-O5	10	-	5	85
BR85-G10-A5	10	5	-	85

First, all constituents were mixed homogeneously according to their respective weight proportions and then each cylinder received a 12 cm layer of its amended bauxite residue on top of the sand layer. Finally, glass beads 3mm in diameter were placed on top for homogeneous distribution of water upon water addition (Stubhaug, 2022).

Acai is a palm species with reddish-purple berries native to northern area in Brazil. The waste of this berry production consists of the seed that remains after pulp extraction process. The acai waste used in that study was provided by Ecobiomassa, a local acai natural pellet producer near Barcarena. After collection the waste was air dried in the laboratory. The food waste used in that study was also produced locally in the region and was mixed and dried at 100°C before storage. Table 3-2 shows the pH, EC and chemical composition of different material used in the mixtures (V. S. Quinteros, 2023).

Table 3-2. Some of the chemical properties of the material used in column leaching test.

Materials	pH	EC	Tot. C	Tot. N	C/N	Na	Al	P	K	Ca	Fe	V	As
		dS/m	(%)	(%)		(g/kg)	(g/kg)	(g/kg)	(g/kg)	(g/kg)	(g/kg)	(mg/kg)	(mg/kg)
Bauxite residue	12.3	3.5	*	*	*	63.0	94.0	0.2	0.1	7.7	190.0	490	16.0
Gypsum	7.3	2.2	*	*	*	0.1	1.4	0.0	0.4	116.7	0.84	2.87	0.36
Food waste	5.2	4.75	50.7	5.5	9.2	6.3	0.1	8.6	7.0	14.0	0.06	0.06	0.04
Acai waste	5.3	1.4	46.2	1.0	44.5	0.0	0.3	0.8	3.1	0.6	0.26	0.44	0.05

3.1.2 Leaching test

To improve the chemical properties of the amended BR prior to ryegrass (*Lolium*) seeding, a total 2360 ml of distilled water was added to the cylinders for 6 weeks (150 ml every third day) to achieve a L/S of 10. Each cylinder contained 236 grams of total dry mass. Leachates were collected and analyzed for concentrations of Na, Ca, K, and Mg using an Agilent 4100 microwave plasma atomic emission spectrometer (MP-AES). In addition the EC , pH and dissolved organic carbon (DOC) of the leachates were analysed using a Metrohm 712 conductometer, a PHM210 standard pH meter, and a TOC analyser, respectively (Stubhaug, 2022).

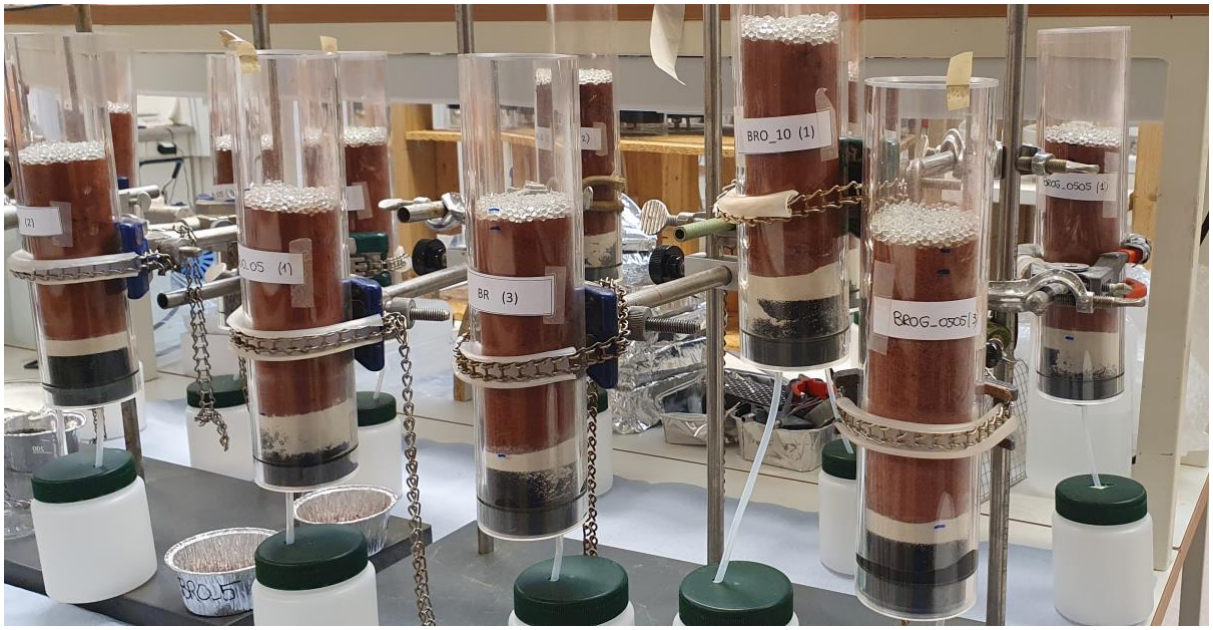

Figure 3-1. Column leaching test prior to seeding at NGI. Measurements of pH, EC, Alkalinity, Ca, Mg, Na, K, DOC, Sodium adsorption ratio (SAR) at liquid to solid ratio of 1 to 10. Image credits: Hogne Phillips Stubhaug.

3.1.3 seeding

Following the leaching process, the glass beads were removed from the top surface, and 30 ryegrass seeds were evenly distributed into the top one centimeter of the mixtures.

Ryegrass is an introduced species to and widely distributed in Brazil, known for its effectiveness in revegetation of amended BR in Ireland (Courtney & Mullen, 2009-b). The columns were then transferred to a climate room at the laboratory in NMBU, where they were kept at a constant temperature of 21°C and were provided with 18 hours of light per day. During the first week after planting, the top layer was sprayed gently with distilled water to prevent flooding the seeds while keeping them from drying out. Once the grass had emerged, more water could be added as needed (Stubhaug, 2022).

3.2 Micro CT scanner

For the current study, one out of three replicate columns (in total 5 out of 15), for each treatment described above, were used for further analysis of the root growth using image processing techniques. To obtain the 3D µCT images, the Nikon Metrology XT H-225 LC located in NGI headquarter in Oslo, Norway was used. The generated X-ray beams are polychromatic. The maximum voltage that can be used is 225 kV and the maximal current was 500 µA. The detector panel has 4.2 Megapixels (2880 x 2880 active pixels with pixel size of 150 µm) and its size is 450 mm x 450 mm. The position of the specimen is controlled by a mechanical arm with reference to the X-ray source and the detector panel. This makes remote zooming possible. The source of scanner allows a minimum voxel size of 3 µm, which implies that in theory, almost all silt particles could be observed. Nonetheless, the geometry of the scanned object determines the spatial resolution (voxel size) that can be achieved. The voltage and current used to scan the cylinders were 150 kV and 120 µA respectively with a 1 mm thick copper filter. The voxel size obtained in this study was 37.8 µm which rendered identification of roots thicker than 0.04 mm. Beam hardening were corrected on the 3D scans.

The five cylinders with different mixtures of amendments and BR were scanned before seeding, after two-, and four weeks following the seed plantation. Image analysis techniques were used on the 3D µCT scans to obtain quantitative information about the ryegrass root system development. Images taken before seeding were analyzed for porosity and those taken after two weeks of growth had been analyzed for both porosity and root features, by NGI prior to the current study. The images from 4 weeks after growth were analyzed for both porosity and root features in this study. Results from before seeding, and two weeks after seeding, were utilized in this study to detect the changes in porosity and ryegrass root growth with time.

3.3 Image analysis

The thousands of radiograms obtained from CT scanning were reconstructed using the FBP technique to a 3D volume using the software VG-Studio Max (volumegaphics.com) as shown in Figure 3-2. The image analysis steps included: preparation, filtering, enhancing and binarization of the roots for data analysis. The latter was done using the opensource ITK-SNAP software (Yushkevich et al., 2006). The programming language Python was used for implementing codes for the data analysis using different packages including `Porespy` (Gostick et al., 2019).

The binarized images; the segmented roots and binarized raw images of bulk soil, were analyzed though a series of algorithmic steps to calculate the descriptive parameters listed below:

- Average root depth (RD in mm), which is the average of the depths of all roots in each column.

- Root Volume Density (RVD in %), which is the total volume of the root divided by the volume of the soil in which the root has permeated.
- Root Area Ratio (RAR in %), which is the surface of the soil permeated by the roots divided by the total area of the soil in which the root has permeated.
- Soil porosity and its changes during development of root features over time.

The soil´s porosity was calculated from the binary 3D images using the formula below:

$$n_{CT} = \frac{N_t - N_s}{N_t} \qquad [7]$$

where:

n_{CT} = porosity based on CT images, N_t = is the total number of voxels and N_s = is the number of voxels of the solid particles on a 3D μCT scan.

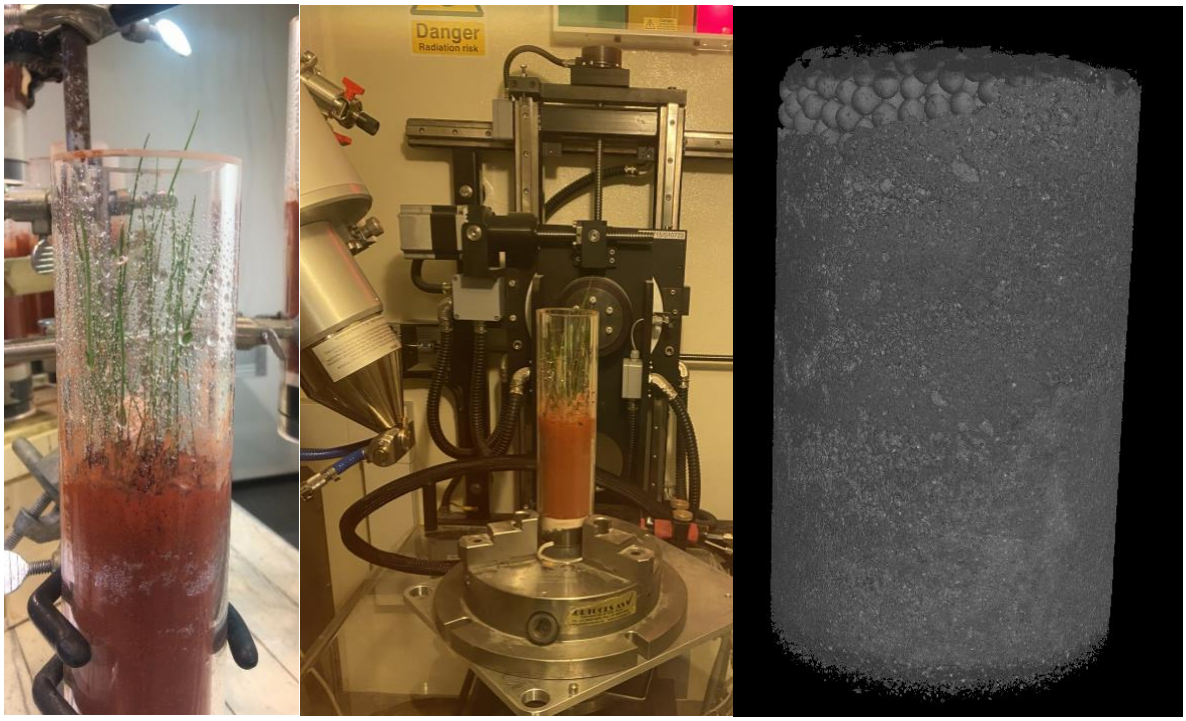

Figure 3-2. from left to write: Ryegrass growing inside cylinder. CT scanning at NGI, the column rotates while repeatedly being imaged from many angles. Reconstructed 3D image of the revegetated BR which can be shown as cross-sectional slices. From (V. S. Quinteros, 2023).

3.3.1 Root segmentation

There are various approaches to do soil-root system segmentation such as region growing (planting a virtual seed inside an object that grows up to the volume of that object), and deep learning to segment the roots in semi-automatic or fully automatic fashion. The main challenge with using these techniques is that over-segmentation and under-segmentation are likely to happen due to the overlapping X-ray attenuation values of the root system with the soil´s organic matter and minerals. The samples in this study, which were amended with food waste, acai seeds, and gypsum and had complex structures including soil aggregates, air-filled pores, and water, presented an even greater challenge as it is shown Figure 3-3. To ensure high precision and accuracy, the root segmentation was done

manually using ITK-SNAP, an off-the-shelf software originally developed for analyzing medical CT-images. The manual process was extremely laborious and required 1-4 weeks for each image depending on the number of roots present. The use of an ergonomic mouse and ITK-SNAP´s keyboard shortcuts were critical to streamline the process.

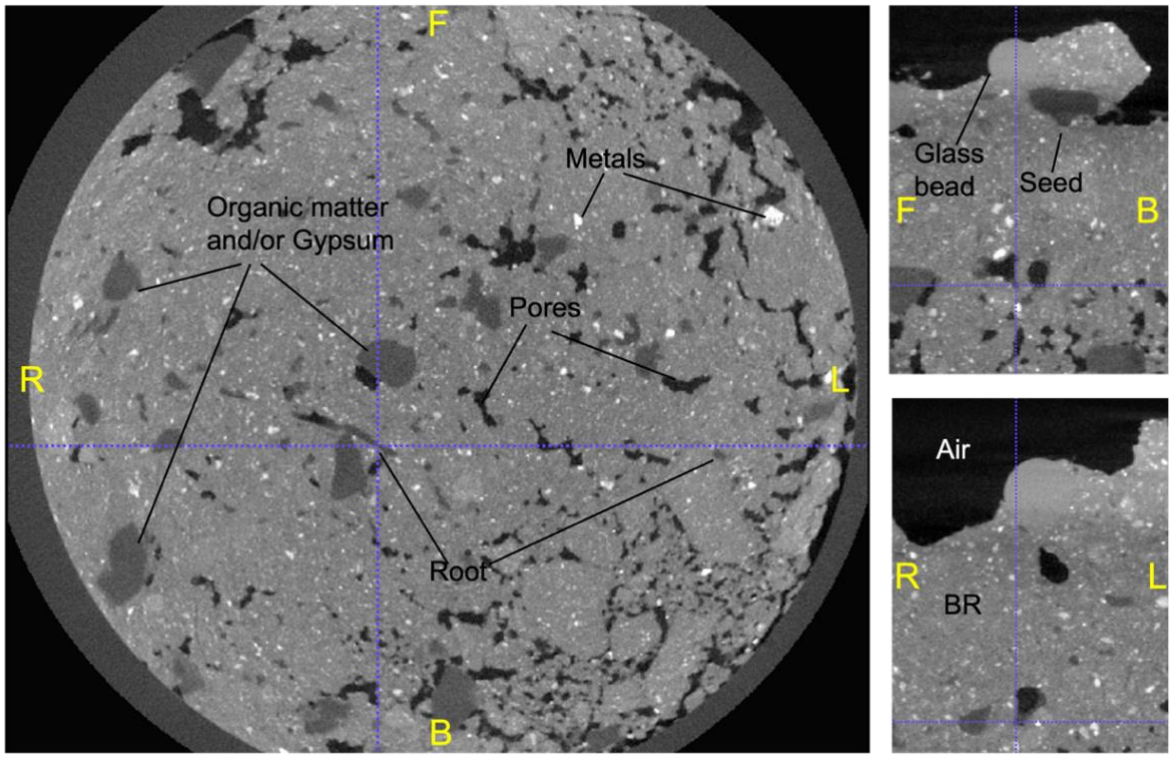

Figure 3-3 Various elements of the amended BR are shown in one of the horizontal cross-sections on the left and the corresponding longitudinal (top) and frontal (bottom) cross-sections on the right. The blue cursor points to the same root in all three slices. R: right, L: left, F: front, B: back.

After auto-enhancing the image contrast using the ITK-SNAP software, the 3D spherical brush tool was utilized to manually segment root regions in over 3000 slices per µCT-scans. Each slice is a greyscale 2D cross-sectional view of the soil profile as shown in the Figure 3-3. Three sets of slices (horizontal, longitudinal, and frontal) were collected per cylinder. The root system appears as smooth elliptical regions in the 2D slices (Mooney et al., 2012). By displaying the slices in Figure 3-3 from top to bottom as a video, the continuous motion of the roots could be observed. This approach provided a reliable basis for root identification and prevented the mis-segmentation of non-root elements in soil environment.

The process of segmentation involved tracking and brushing each root while adjusting the brush size to match the root diameter. Individual primary roots were segmented starting from the soil-air interface to the bottom of the cylinder, followed by segmenting the corresponding lateral roots. Whenever a root was discontinued in one plane, the two other planes were inspected for changes in root´s spatial direction. There were two visual signs for differentiate roots from organic material. The specific elliptical shape of the roots, and the continuity/mobility of the roots in the soil which could be seen by scrolling through slices. The organic material mostly didn't have elliptical shape and they were stagnant in the image (they would disappear with scrolling). The 3D volume of the roots obtained in

this step were exported to python for further analysis and computation of root descriptors. To see the ITK-SNAP´s interface see Figure 10-1.

3.3.2 Calculation of descriptive petameters

The outcome from image segmentation process were binary three-dimensional arrays in TIF format. These arrays, which are three dimensional matrices, are numerical representation of the root volume. For instance, the size of the segmentation volume of BR90-G5-A5 was 1898 x 1352 x 1355, indicating the number of voxels in the X, Y, and Z dimensions. The value of each of these voxels was either 0 or 1 representing the space occupied by no-root (nothingness) or root, respectively.

The calculation of the porosity was done using the unsegmented greyscale three-dimensional images (raw 3D images) where the values in the arrays ranged from 0 to 256. The process of calculating the descriptive parameters is summarized in Figure 3-4.

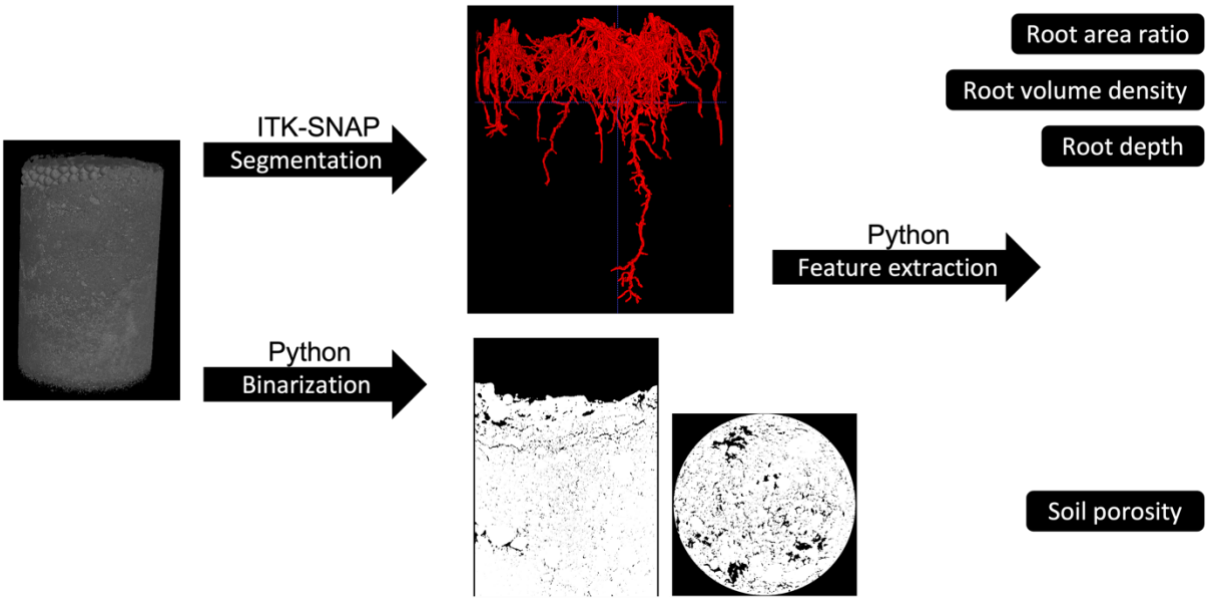

Figure 3-4. Schematic diagram of the general steps in the image processing. Thousands of cross-sectional slices can be accessed from the reconstructed 3D image to segment the roots out. The raw image is binarized for quantifying soil porosity.

The segmentation volumes were used to count the roots and calculate root depth, root volume density, and root area ratio. An average starting point (Y value) of all the roots for each cylinder was calculated. This value was then subtracted from Y value of each root tip to obtain root depth in voxels which was converted to mm using the image's voxel size (37.8 µm). Root volume density of the roots were calculated by summing up all the voxels, converting to mm and then dividing by volume of the root-permeated soil.

$$RVD\ \% = \frac{solid\ volume\ mm^3}{A * mean\ RD} * 100 \qquad [8]$$

`Porespy` is a set of tools for analyzing 3D images of porous materials obtained from X-ray tomography. It simplifies the process by providing predefined functions specifically designed for porous media analysis. Unlike other general image analysis packages like `skimage`, `scipy.ndimage`, which require complex scripts or macros to perform tasks specific to porous materials, `PoreSpy` offers ready-to-use functions for routine analyses, making the process faster and more convenient (Gostick et al., 2019).

RAR was calculated by summing up the root-permeated fractions of soil cross-sections in the root segmentation volume. This was done using package `porosity_profile` which went through the vertical axis of each column and calculated the surface area occupied by root relative to the total area of the horizontal cross-section.

The process of calculating porosity involved converting grayscale raw images to binary images using scikit-images `threshold_otsu` filter, creating a black and white image where air-filled pores appeared black and the solid particles appeared white. The image was then cropped from the top and sides to remove the air space above the soil and the transparent walls of the cylinder. The side-cropping part was done by defining a cylindrical 3D mesh around the specimen and removing everything outside it. The diameter of the mesh was gradually reduced to eliminate distortion at the wall-soil interface as it is shown in the Figure 3-5. Finally, the cleaned and filtered image was analyzed for porosity using the `porosity_profile` package.

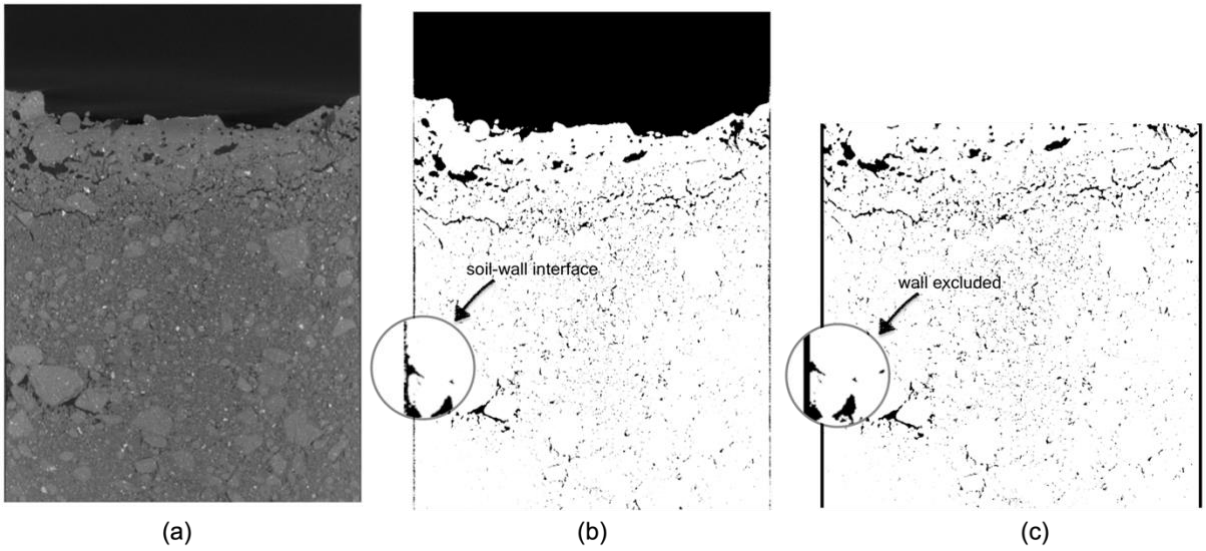

Figure 3-5. The steps in preparing and thresholding the raw image before measuring the porosity profile. (a) the raw image. (b) is the binarized image. (c) is the cropped image with column wall and air above the cylinder excluded. The clear sharp edge is the sign that we are inside the column wall.

3.4 Principal Component Analysis (PCA)

PCA is a dimension reduction method and is used to decompose a multivariate dataset to fewer number of new components which explain the maximum amount of variance in the dataset (scikit-learn, 2023). These new components are called principal components or latent variables. In this study, the chemical dataset obtained in (Stubhaug, 2022) was used for PCA in order to gain insight to the chemical state of the mixture and to link it to image analysis results for roots. Furthermore, PCA shows the correlation of different measured parameters with each other.

In short, the raw data, an Excel file containing several sheets, that was kindly shared by Stuhbhaug (2022), was cleaned and restructured as follows. The 9 different parameters for the 5 X 3 (mixture times replicates) samples for L/S 1 and 10 were collected and gathered in one table. The multivariate datasets with 30 rows (samples) and 9 columns (variables) is shown in Table 3-1. Some of the measurements for DOC and Mg were originally <LOD and they were replaced by values that would least affect the variance in

the data. The three <LOD cells of the DOC column were replaced by the average of the column because i) LOD value was unavailable ii) the average of the column (103 mg/L) was much higher than the minimum value (16 mg/L), suggesting most values were high and that '<LODs' were more of an experimental/instrumental error than a low concentration. The <LOD cells of the Mg column were replaced by the low value 10^{-5} because i) the LOD was available (0.00246 mol/L) ii) other values were in average low (min = 0.01481, mean = 0.07940, max = 0.32092 mol/L). Additional substitution attempts were made by replacing the minimum of the column for DOC unknown values and the (LOD/$\sqrt{2}$) for unknown Mg values, but the PCA results were no different (data not shown here).

The PCA was done in Python using `sklearn.decomposition` package after scaling the data with `sklearn.preprocessing` due to unit non-uniformity. Colors and shapes were pre-assigned to the data points according to their mixture type and L/S, respectively. Four components were used for PCA as they explained over 80% of the variance, out of which the first two were visualized which explained ~70% of the variance. K-means clustering analysis, a classification method based on the principle that "things that are close together are probably similar", was done using `sklearn.cluster` and optimal number of clusters using elbow method (Lervik, 2023). The first was done on the whole dataset shown Table 3-3. Then a second PCA was done on half of the data only for measurements from L/S 10 which was important as it explained the chemical condition of the mixture before vegetation establishment.

There were two sets of plots for visualizing each PCA: scores and loadings. Scores are the coordinates of each sample in the new latent axes (PC1 and PC2) and are used to see interesting patterns, clustering of datasets, and detect outliers. Loadings tells us about how important each variable is in describing the direction of a latent variable. Loading are used to detect correlated variables by looking for clusters, which variable contribute more to each principal components, negatively correlated variables which are at opposite locations along a PC, and unimportant variables for the model which are situated close to the origin (Lervik, 2023).

After the results from calculation of root descriptors were obtained, a third PCA was performed in order to detect positive and negative correlations between root descriptive parameters and chemical variables of the mixtures.

3.5 Statistical analysis

To examine linear relationships and correlations between root descriptors and chemical parameters, a linear trendline was fitted into scattered plot of root depth versus their associated number and R-value was registered.

For comparison of pH and EC values between the mixture with either 10% or 5% gypsum content of amendment, a two-way t-test was performed in Microsoft Excel. Normal distribution was assumed because these variables are influenced by numerous statistically independent factors.

Table 3-3. The data that was used for the PCA analysis.

Samples	pH	EC (dS/m)	Alkalinity (mmol/L)	DOC (mg/L)	SAR	Ca (mEq/L)	Mg (mEq/L)	Na (mEq/L)	K (mEq/L)	L/S
BR90-G10-1	9,24	2,1	0,37	490	6	27,45	0,00001	22,18	0,02	10
BR90-G10-2	8,74	2,1	0,32	103	6,1	26,45	0,00001	22,18	31,17	10
BR90-G10-3	8,75	2,12	0,54	103	6,2	26,95	0,00001	22,62	0,02	10
BR85-G10-A5-1	8,55	2,27	2,11	103	7,9	26,45	0,00001	28,71	117,54	10
BR85-G10-A5-2	8,48	2,44	1,10	16	7,7	27,95	0,00001	28,71	0,02	10
BR85-G10-A5-3	8,04	2,88	1,67	16	23,1	22,96	0,05349	78,29	301,51	10
BR90-G5-A5-1	9,61	0,804	4,47	19	76,9	0,38	0,00001	33,49	0,00	10
BR90-G5-A5-2	9,40	0,81	2,90	38	12,8	7,98	0,02222	25,66	1297,62	10
BR90-G5-A5-3	9,11	0,805	2,40	22	61,4	0,55	0,00001	32,19	0,00	10
BR85-G10-O5-1	7,48	2,03	1,50	99	12	26,45	0,03456	43,50	3008,13	10
BR85-G10-O5-2	7,49	2,45	0,85	180	9,1	22,46	0,01481	30,45	0,00	10
BR85-G10-O5-3	7,60	2,09	3,95	120	15,9	13,47	0,08229	41,32	4512,19	10
BR-90-G5-O5-1	8,36	0,966	1,80	140	35,8	0,40	0,00001	16,09	0,00	10
BR-90-G5-O5-2	8,34	1,2	4,11	37	16	1,25	0,00001	12,61	3814,85	10
BR-90-G5-O5-3	9,21	0,647	5,08	61	19,3	0,80	0,00001	12,18	0,00	10
BR90-G10-1	9,26	5,3	2,71	410	306	36,43	0,01563	1304,92	2,40	1
BR90-G10-2	9,42	5,2	2,90	300	208	38,43	0,02386	913,44	1,87	1
BR90-G10-3	9,84	4,9	2,42	370	337	38,43	0,02633	1478,90	2,40	1
BR85-G10-A5-1	9,35	4,7	5,69	170	261	43,42	0,06089	1217,92	6,14	1
BR85-G10-A5-2	9,03	4,6	5,73	370	231	40,92	0,11520	1043,93	6,91	1
BR85-G10-A5-3	8,86	4,7	3,69	230	230	34,43	0,08146	956,94	5,12	1
BR90-G5-A5-1	8,81	4,7	6,10	680	348	33,93	0,02798	1435,41	5,63	1
BR90-G5-A5-2	8,11	5,7	1,44	430	348	24,45	0,05102	1217,92	4,60	1
BR90-G5-A5-3	7,99	5,4	3,56	620	282	39,92	0,04855	1261,42	6,14	1
BR85-G10-O5-1	6,86	5,5	3,09	3700	109	45,41	0,09875	521,97	2,56	1
BR85-G10-O5-2	6,15	6,5	1,67	2300	50,2	79,84	0,26332	317,53	2,25	1
BR85-G10-O5-3	6,29	5,9	2,27	1800	50,4	74,85	0,09875	308,83	2,20	1
BR-90-G5-O5-1	8,81	12,03	2,74	3700	114	64,87	0,32092	652,46	3,84	1
BR-90-G5-O5-2	8,11	10,66	2,32	2300	154	26,95	0,07900	565,46	2,17	1
BR-90-G5-O5-3	7,99	13,5	2,65	4200	135	59,88	0,06912	739,45	4,09	1

4 Results

Figure 4-1 displays cross-sectional views of the upper portions of cylinders that contains various mixtures of bauxite residue after four weeks of growth. It is important to observe the distinct shades of gray representing clusters of bauxite residue, organic food waste, acai seed waste, and roots. Note the apparent different pore and aggregate distribution in different mixtures. Radiographs in the figure are one cross-section out of thousands and are not representative of the whole space of the bulk soil. The raw 3D visualizations were utilized to compute the porosity, which will be explained in detail below.

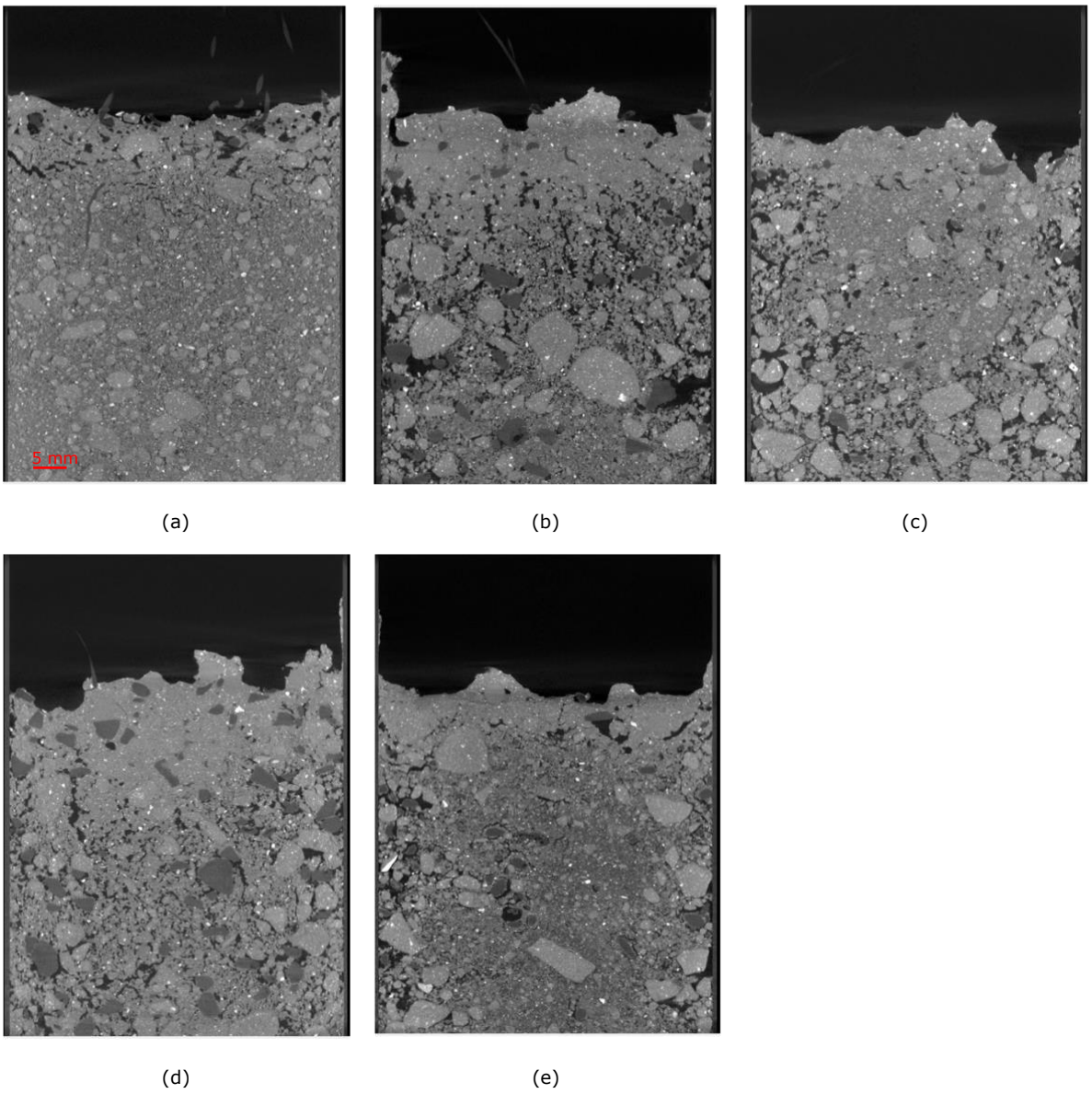

Figure 4-1. µCT scans of the top 6 cm of bauxite residual mixtures after four weeks of growth: (a) BR90-G10; (b) BR85-G10-A5; (c) BR85- G10-O5; (d) BR90-G5-A5; (e) BR90-G5-O5.

4.1 Segmented roots

A 2D representation of three-dimensional segmentation volumes from the roots that were developed in 4 weeks are shown in Figure 4-2. These volumes were manually segmented

from the raw images that are shown in Figure 4-1. BR90-G10 (Figure 4-2 a) had a dense and spatially homogenous root formation in the top layer with thicker roots compare to other amendments (Figure 4-2-a). Many lateral roots can be seen at all depths in this amendment.

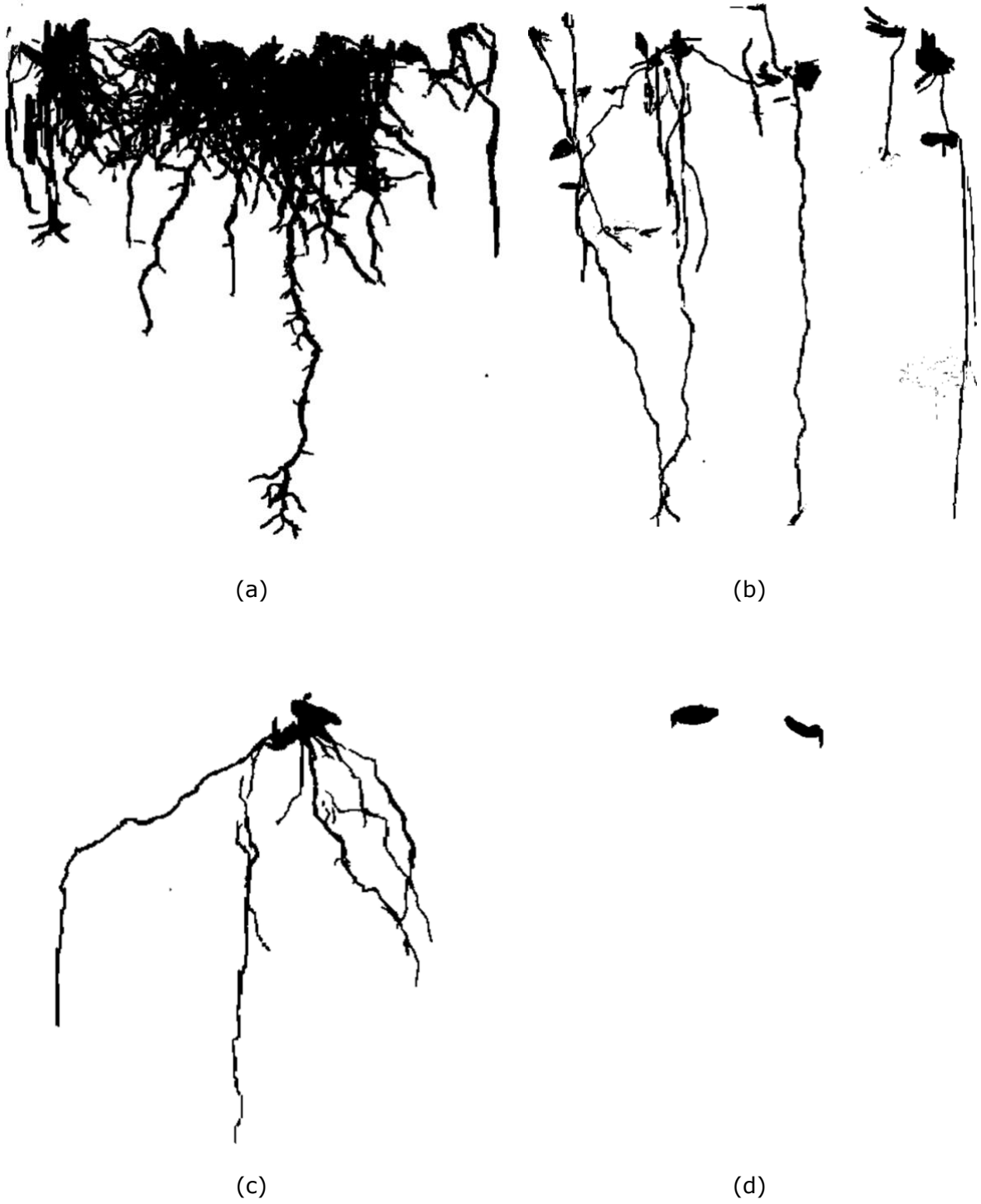

Figure 4-2. Snapshots of the 3D segmented root volumes from different mixtures after 4 weeks of growth. (a) BR90-G10. (b) BR85-G10-A5. (c) BR85-G10-O5. (d) BR90-G5-A5. No roots were observed in BR90-G5-O5. Note that the segmentation has been done from the soil-air interface downwards and that the root-growing seeds are also segmented.

The root growth BR85-G10-A5 (Figure 4-2c) was less spatially distributed as it could be characterized by mainly long, thin, and straight primary roots, with some lateral roots at lower depths (Figure 4-2-b). In addition, they were considerably distanced from each other. The roots of BR85-G10-O5 (Figure 4-2 d) on the other hand, showed more of spatial growth while being limited to thin and primary roots Figure 4-2-c). BR90-G5-A5 and BR90-G5-O5 showed very little and no root growth, respectively (Figure 4-2-d).

4.2 Root number and depth

The number of the roots developed in each soil amendment and their depths after two and four weeks of growth are shown in Figure 4-3.

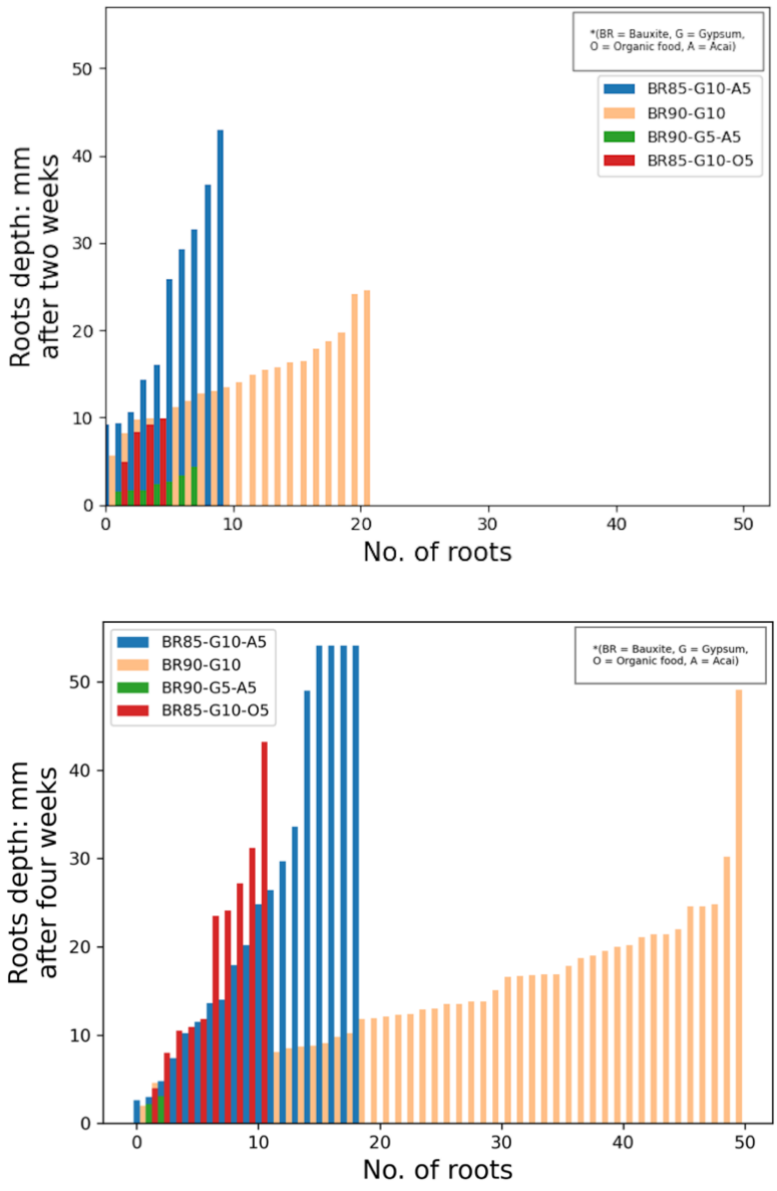

Figure 4-3. Number of roots that was observed in each mixture type from 30 seeds after two (top), and four (bottom) weeks of growth, with their associated depths. BR90-G5-O5 is not shown in the plot because there were no roots developed in that mixture.

After two weeks, the maximum number of roots, 21, were found in BR90-G10 followed by BR85-G10-A5, which had developed 10 roots. Seven (7) roots were observed in BR85-G10-O5, and only 4 short roots were seen in BR90-G5-A5. No roots were observed for BR90-G5-O5. The maximum root depth was 42.9 mm and was seen in BR85-G10-A5.

After four weeks, the maximum number of roots, 50, were found in BR90-G10 followed by BR85-G10-A5, which had developed 18 roots. Ten (10) roots were observed in BR85-G10-O5, and only a couple of short roots were seen in BR90-G5-A5. No roots were seen in BR90-G5-O5. The relationship between root depth and root number for BR90-G10, up to the depth approx. 22 mm, was linear with R^2 = 0.98 and the slope of 0.4, indicating that a root was present at each 0.4 milliliter depth. However, only a couple of root-tips were seen in the depth range 30-45 mm across all amendments which indicates some kind of stress (e.g., nutritional, water, gas) at those depths. The maximum root depth was 54.1 mm and belonged to BR85-G10-A5.

4.3 Root depth (RD)

Figure 4-4 shows the average and maximum RD for each amendment after two and four weeks of growth. The average RD for BR90-G10 remained the same, 14.5 mm, while the maximum value increased noticeably from 25 to 49 mm. On the other hand, both average RD and the maximum RD of BR85-G10-O5 increased noticeably from 8 to 19 mm, and from 10 to 43 mm, respectively. The average RD had stayed 3mm for BR90-G5-A5 from second to fourth week. This was not the case for BR85-G10-A5 as the average RD had increased from 23 to 26 mm while the maximum RD had increased from 43 to 54 mm. In both two and four weeks after seeding, the BR85-G10-A5 amendment has the deepest root whereas BR85-G10-O5 had exhibited the greatest increase in the depth to which roots had permeated.

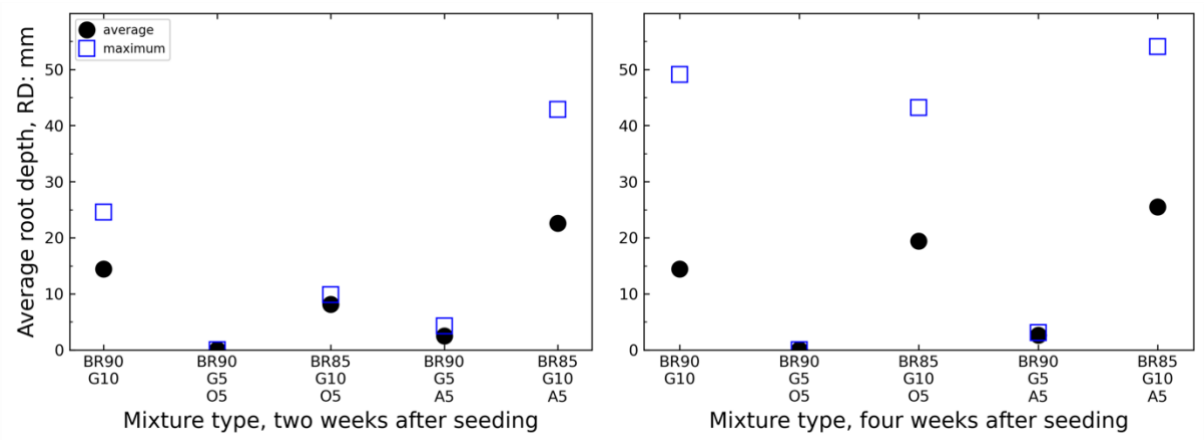

Figure 4-4. Average root depth (shown in black filled circles) and maximum depth of the roots (blue hollow squares) in each mixture type after two (left) and four (right) weeks of growth.

4.4 Root volume density (RVD%)

Figure 4-5 depicts the volume density of the roots with respect to average root-permeated depth, and not the total volume of the cylinder, in each mixture type. Among the amendments, BR90-G10 has the highest RVD of 0.5 and 2.3% both in the two and four weeks after seeding. This amendment has also shown the highest increase from the second to the fourth week.

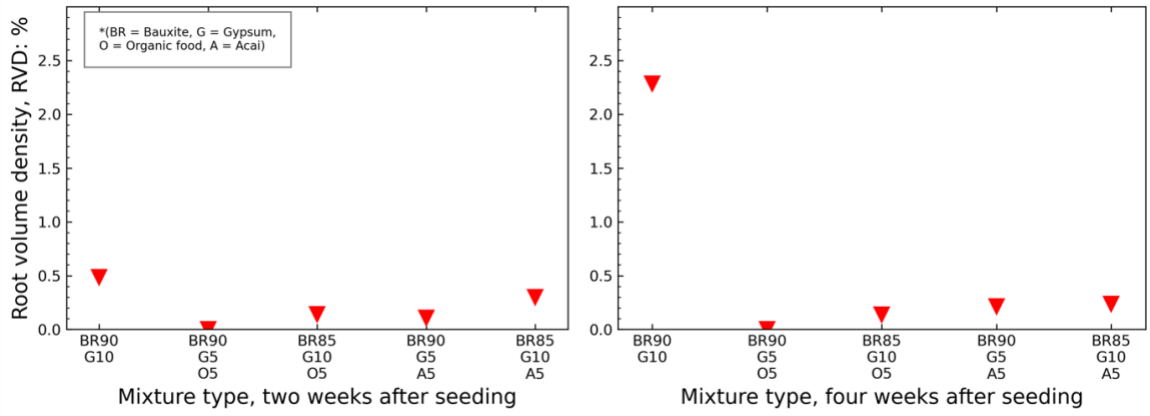

Figure 4-5. Root volume density in different mixture types after two (left) and four (right) weeks of growth.

The BR85-G10-A5, with considerable difference, had the second highest RVD% with a slight decrease from the second to the fourth week. It can be noted here that after four weeks the BR85-G10-O5, though has developed more root material, has a lower RVD% than BR90-G5-A5 simply because of having a larger average root-permeated depth (larger denominator in equation 8). Therefore RVD% alone should not be considered a decisive attribute and should be interpreted aside other descriptors.

4.5 Root area ratio (RAR %)

The RAR was calculated per depth down to the lowest depth into which the roots had penetrated. Here, the RAR% values after two- and four-weeks after seeding are shown in Figure 4-6. It is important to mention that most of the seeds were planted in the top 10 mm of the soil. Since the living seeds were also segmented along with the roots, not all RAR values in that depth range necessarily correspond to the roots. However, the RAR values are comparable as only those seeds which developed roots are included in the plot in each column. The RAR profiles of all amendments show the same trend. They reach a peak in shallow layers and then decrease with depth. This is typical of grass species, where usually most roots are observed in the shallowest layers, tending to decrease exponentially with depth (Foresta et al., 2020).

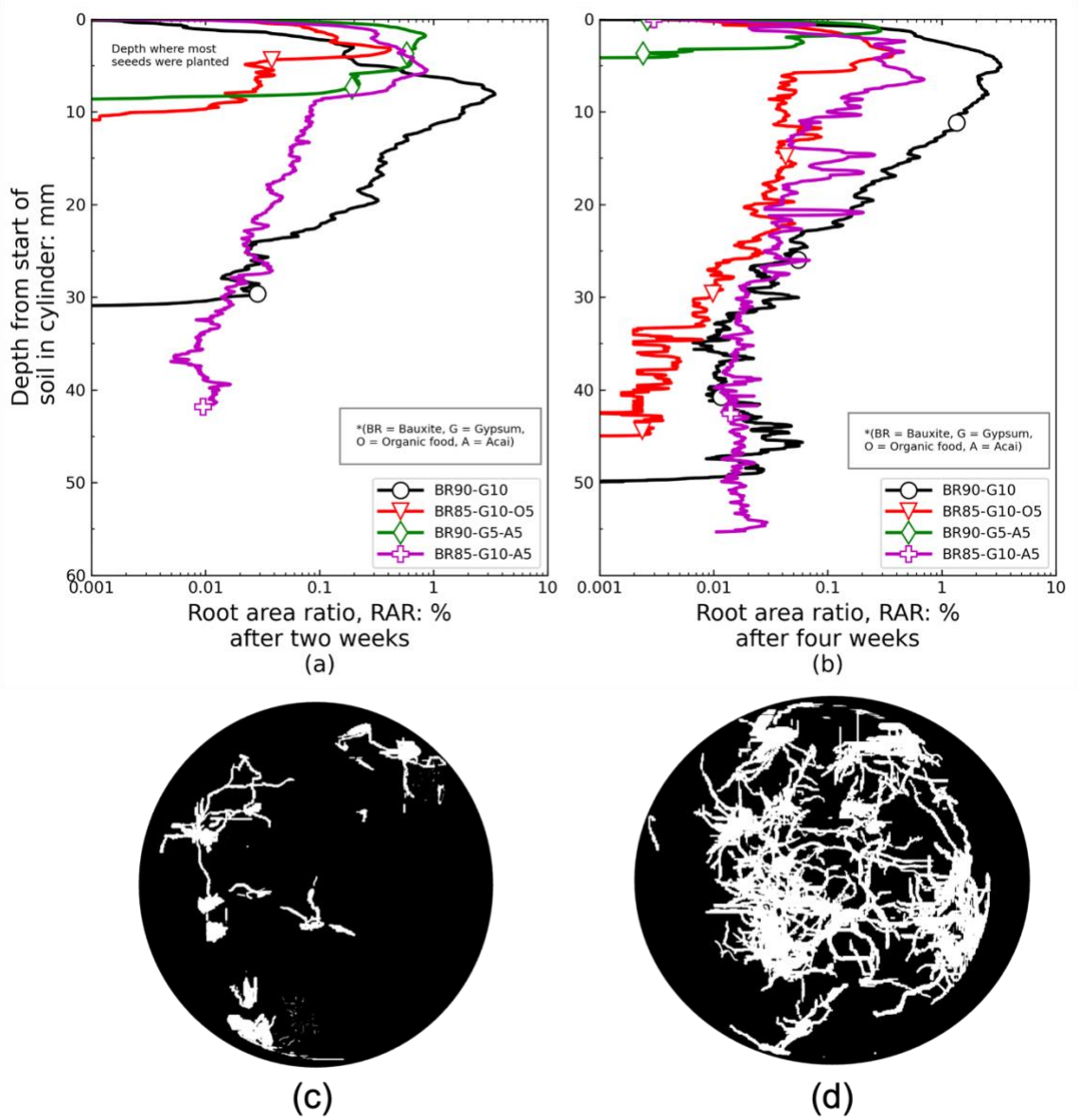

Figure 4-6. Root area ratio after (a) two weeks and (b) four weeks of growth. BR90-G5-O5 is not included in the plot as it had not developed any root. (c) and (d) is the top-view of the segmented root system in BR85-G10-A5 (shown with purple) and BR90-G10 (shown with black) mixture types, respectively. Quantification of RAR is done from the top to bottom; inward in (c) and (d) is same as downward in (a) and (b). Solid parts (roots) are in white and empty space is in black.

Figure 4-6 indicates that the highest RAR value(s) were developed after two weeks with average value of 0.2% and remained so after 4 weeks of growth in BR90-G10 (black) with average value of 0.4%. The second highest and total values were seen in BR85-G10-A5 (purple) after 2 weeks of growth (in average 0.01%) and were closely shared between BR85-G10-A5 (purple) with the average value of 0.06% and BR85-G10-O5 (red) with the average value of 0.03%, after 4 weeks of growth. The latter had shown a noticeable increase in RAR at depths between 10-50 mm while the former had developed roots in the deeper layers. It´s worth noting that the BR90-G5-A5 mixture was the only one that showed a decrease in RAR value(s) from the second to fourth week. This could be due to microbial degradation by alkaliphilic microorganism who grow preferentially in the high moisture content soil. There was already little amount of root in this mixture with low structural integrity which in turn means less water uptake, more moisture accumulation in soil, and easier breakdown of roots by microbes. The BR90-G5-O5 was the worst amendment among all in terms of root development with no roots observed whatsoever.

In the fourth week plot sudden increases can be seen for instance between the depth 15 to ~30 mm for the purple line or the depths 30 and 45 mm for the black line. These signal increases are caused by lateral root growth and branching in the case of 20 to ~30 mm depth for the purple and the black. However, the sudden increases in 15-20 mm depth of purple line are caused by the mis-segmentation of acai seeds as some parts of them were coarse and hard to differentiate from roots due to their elliptical shapes. This has been registered by comparison of the images in Figure 4-2 and Figure 4-6-b and visually establishing relationship between the picks on the plot and corresponding elements in the root image (not shown here). Note that lateral roots in the top layer are embedded into the logarithmic scale especially for the black line which had the most laterals in those depths (see Figure 4 2-figure 4-2-a). On the other hand, sudden increase-decrease patterns in all lines are considered as noise and not signal.

4.6 Porosity

The porosity values of the soil mixtures with respect to depth, before seeding, 2 weeks and 4 weeks after seeding, are depicted in Figure 4-7.

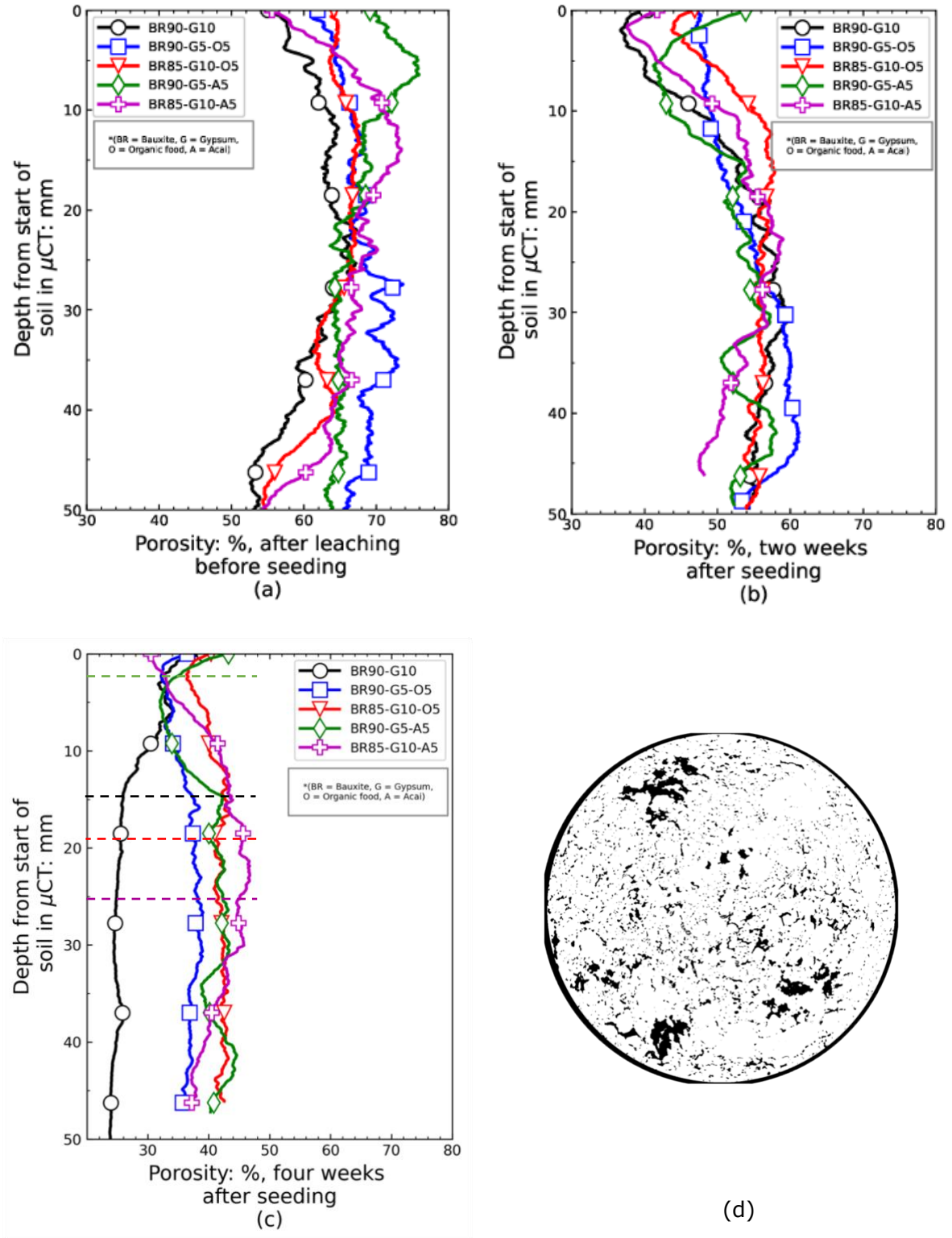

Figure 4-7. Vertical porosity% profiles in all 5 mixture types (a) after the leaching/before seeding (b) two weeks after and (c) four weeks after seeding of ryegrass. Dashed lines show the average RDs (d) shows the binarized top-view image of BR90-G10 column as an example (solids: white, pores: black). Porosity quantified top-bottom; inward in (d).

In general, there was a decrease in porosity in all soils after two and four weeks from the seeding. This decrease was characterized by an initial reduction of the porosity in the upper 2 cm of all samples during the first two weeks, followed by a decrease in porosity at lower depths by the fourth week. For BR90-G10 (black line), a noticeable decrease in porosity can be seen at the fourth week, such that after the depth 14.5 mm the porosity remained around 24%. Interestingly, this depth is same as the average root depth for BR90-G10 as shown in Table 4-1. The other 10% gypsum mixtures, red and purple lines, have higher average porosities after four weeks thus roots have penetrated deeper.

Table 4-1 summarizes results from number of roots, RVD, RD, RAR, and porosity calculations for different mixtures before and after seeding. The average porosity in all mixtures has low variability (STD≅1), but porosity varies more (STD=6.1) in the fourth week, especially in mixtures containing 10% gypsum. This indicates the interplay between porosity and root growth. BR90-G10 with the highest amount of root material has the highest porosity variability and is farthest from the mean value, followed by the other two mixtures with 10% gypsum.

Table 4-1. Summary of the measurements.

Parameter	Weeks after seeding	Mixtures of BR and different amendments[1]					STD[6]	mean
		BR90-G10	BR90-G5-O5	BR85-G10-O5	BR90-G5-A5	BR85-G10-A5		
No. roots	2	21	0	4	7	10	7.6	7
	4	50	0	10	2	18	18.8	14
RVD[2] (%)	2	0.5	0	0.1	0.1	0.3	0.2	0.2
	4	2.3	0	0.1	0.2	0.2	1.0	1
RD[3] (mm)	2	14.5	0	8.1	2.5	22.6	9.2	10
	4	14.5	0	19.4	2.7	25.5	10.9	12
RAR[4] (%)	2	0.2	0	-	-	0.01	-	-
	4	0.4	0	0.03	0.006	0.06	0.2	0.01
Porosity[5] (%)	0	65	62	63	65	64	1.3	64
	2	55	54	53	53	55	1.0	54
	4	27	37	42	40	41	6.1	37

[1]BR=Bauxite residue, G=Gypsum, O=Organic food waste, A=Acai. [2]RVD=Root Voume Density

[3]RD=Root Depth (average value of all roots). [4]RAR=Root area ratio (average value of all depths). [5]Mean values of porosity. [6]Sandard deviation. Dash=Data unavailable

4.7 Principal component analysis (PCA)

The results from the PCA are shown in Figure 4-8. The Figure 4-8-a and Figure 4-8-b represent the result from first PCA which was fitted into the chemical data consisting of both pre- and post-leaching of the columns that is L/S 1 and 10. The Figure 4-8-c and Figure 4-8-d show the second PCA results which was done on the post-leaching that is at L/S 10 dataset. The datapoints on scores plots in both of the above are triplicates of each mixture. The colors are consistent with the colors used in Figure 4-6 and Figure 4-7 for the same mixtures.

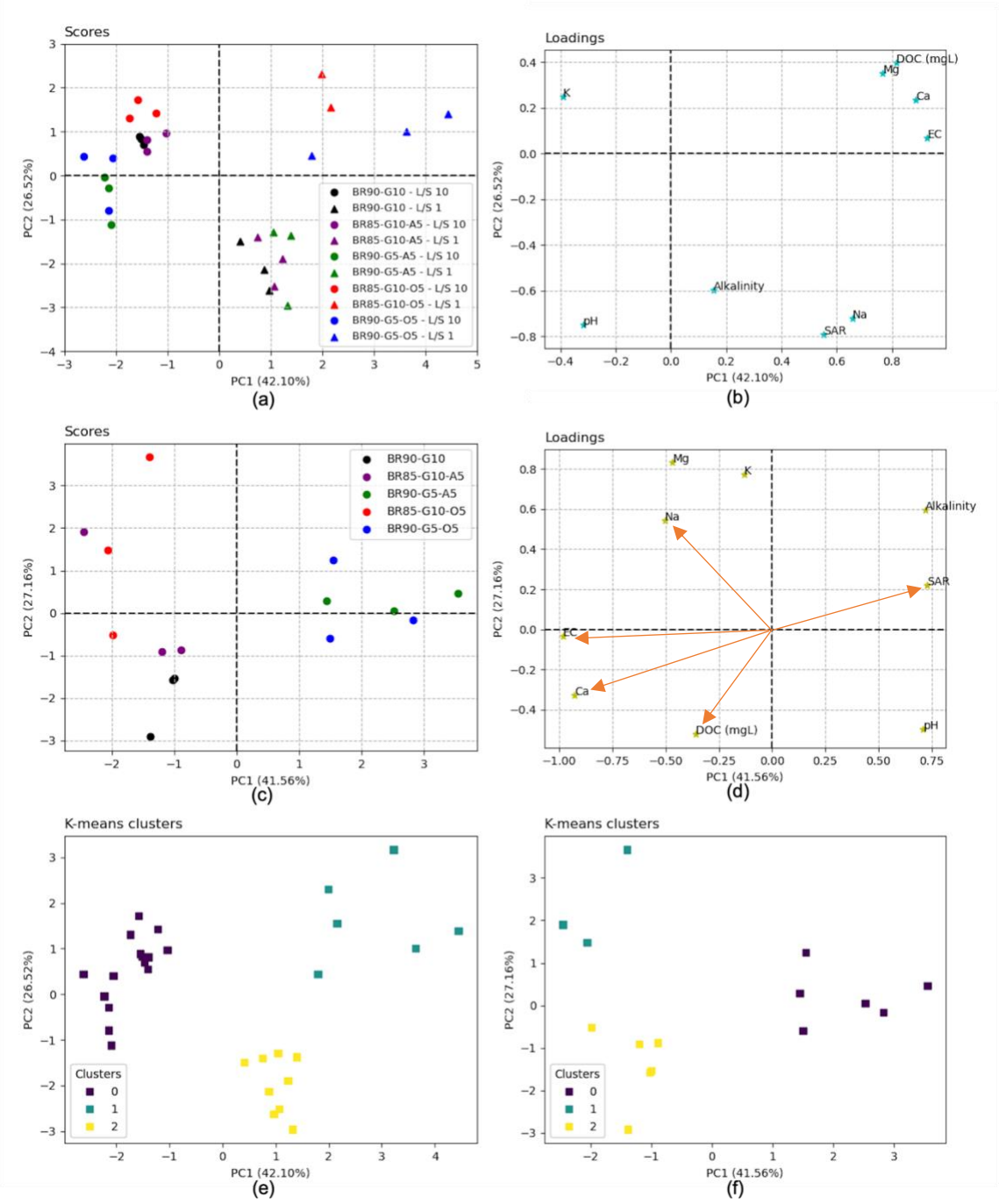

Figure 4-8. The PCA of the chemical data. (a) Score plot for all samples at L/S of 1; pre-leaching and 10; post-leching. (b) Loadings plot for all samples at L/S of 1 and 10. (c) Score plot for all samples at L/S of 10. (d) Loadings plot for all samples at L/S of 10. (e) Results of the K-mean cluster analysis for all samples at L/S of 1 and 10. (f) Results of the K-mean cluster analysis for all samples at L/S of 10. BR: bauxite residue, G: Gypsum, A: Acai waste, O: Organic food waste.

The first principal components (or the first latent variant) in both PCAs described ~42%, and the second PC described ~27% of the variability of the pre- and pro-leaching data. There is a clear separation along PC1 axis between chemical properties of mixtures before and after leaching which are shown with circles and triangles, respectively. Furthermore, prior to leaching the mixtures can be grouped according to the type of organic material used for the amendment; acai or food waste, and the mixture with only gypsum can be

also grouped with the mixture with the ones with acai (along PC2 in Figure 4-8-a). However, after leaching the mixtures can be grouped together according to the weight proportion of gypsum and/or BR (Figure 4-8-c).

When examining the loadings, we can see that both before and after leaching (Figure 4-8-b, and -d), the EC had the most pronounced effect on variability/grouping of the samples, expressed by PC1, followed by the Ca, DOC, and Mg concentrations. The angle between each variables vector shows their association with each other (Figure 4-8-c). Angles of <90°, >90°, =90° depict correlation, anti-correlation, and no-correlation (Lervik, 2023). Given that, we see that prior to planting the seed (Figure 4-8-d), EC and Ca are correlated, and they both are anti-correlated with SAR. Moreover, EC and Ca are more closely correlated than EC and Na. This suggests that Ca contributes more to EC than Na does. In addition, we can see that prior to plantation the influence of DOC contributes relatively little to the overall variability among samples, as the vector that represents it is closest to the origin. Based on this, it is likely that DOC has contributed more with its lability grade (its quality) and less with concentration (its quantity) on the variation root performance variation across mixtures.

The K-mean clustering using 'elbow method' to determine the number of clusters, showed 3 clusters in both PCA scores. In Figure 4-8-f we can see that the non-root developing mixtures (blue and green) clustered together, while BR90-G10 and BR85-G10-A5 triplicates formed the second cluster and except for one replicate, BR85-G10-O5 replicates formed the third cluster.

4.7.1 Root descriptors versus chemical parameters

Another set of principal components was fitted into to the chemical data from after the leaching (L/S 10), this time together with the root descriptors, to see the potential correlations between the chemical parameters and the root descriptors. In the image analysis we had tested one column per treatment hence one value for each root descriptors per treatment was obtained. Therefore, the average of the three replicates for each treatment was used for doing the PCA. The exception was the DOC value for BR90-G10 and BR85-G10-A5 for which the non-'<LOD' values of the replicates in the original data, were used. For the depth-wise root measurements, namely RAR and porosity, the post-leaching average of all depths were used. Likewise, the average value of RD per treatment was used.

Table 4-2. The data that was used to find correlations between root descriptors and chemical parameters.

Samples	pH	EC (dS/m)	Alk. (mmol/L)	DOC (mg/L)	SAR	Ca (mEq/L)	Mg (mEq/L)	Na (mEq/L)	K (mE/L)	RAR%	RVD%	RD (mm)	Porosity%
BR90-G10	8,91	2,11	0,41	490	6,1	26,95	0,000	22,33	10	0,40	2,30	14,50	27,00
BR85-G10-A5	8,36	2,53	1,63	16	12,9	25,78	0,018	45,24	140	0,06	0,20	25,50	41,00
BR90-G5-A5	9,37	0,81	3,26	26	50,4	2,97	0,007	30,45	433	0,01	0,20	2,70	40,00
BR85-G10-O5	7,52	2,19	2,10	133	12,3	20,79	0,044	38,42	2507	0,03	0,10	19,40	42,00
BR-90-G5-O5	8,64	0,94	3,66	79	23,7	0,82	0,000	13,63	1272	0,00	0,00	0,00	37,00

This time 47.62% of the variation in the data was explained by PC1 and 37.65% by PC2. The scores plot showed clear grouping of non-root-developing mixtures together, the two mixtures with 10% gypsum and organic waste together, and the gypsum-only mixture was an outlier (Figure 4-9-a). This is not very surprising because root descriptors were involved in this PCA.

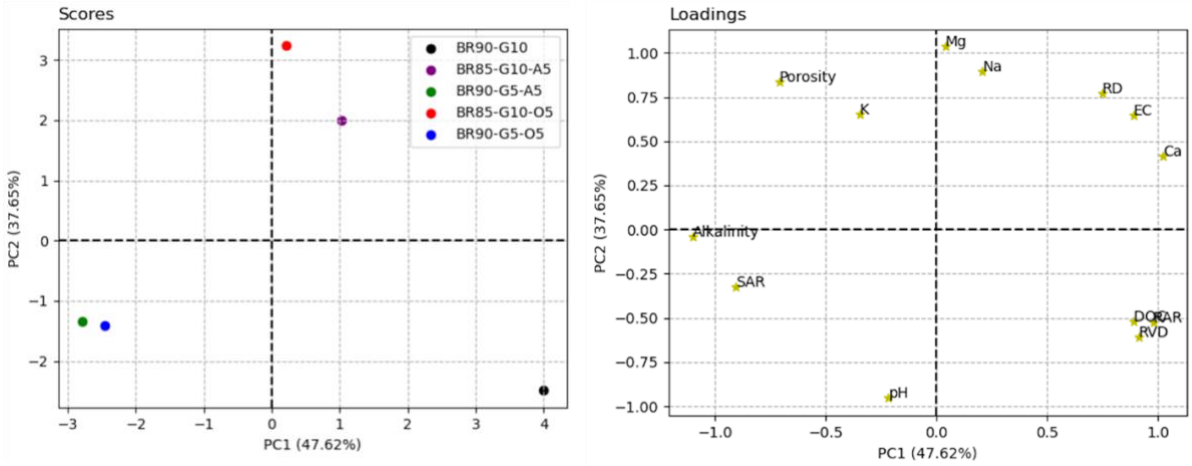

(a) (b)

Figure 4-9. Results from the PCA of chemical data and root descriptors. (a) Scores plot (b) Loading plots of all variables including root descriptors. BR: bauxite residue, G: Gypsum, A: Acai waste, O: Organic food waste.

The apparent correlations shown by the loadings plot were further tested for linearity. The most important ones are shown in Figure 4-10. The order of linear correlation was found to be RD-EC > RVD-DOC=RAR-DOC > RD-Ca > RAR-Alkalinity > RVD-Alkalinity. The correlations that are found between RAR and RVD with DOC (RVD-DOC, and RAR-DOC) should be interpreted with caution because the datapoints are not spread along the horizontal axis that much and the correlation is due mainly to the existence outlier. On the other hand, RD-EC is a reliable correlation.

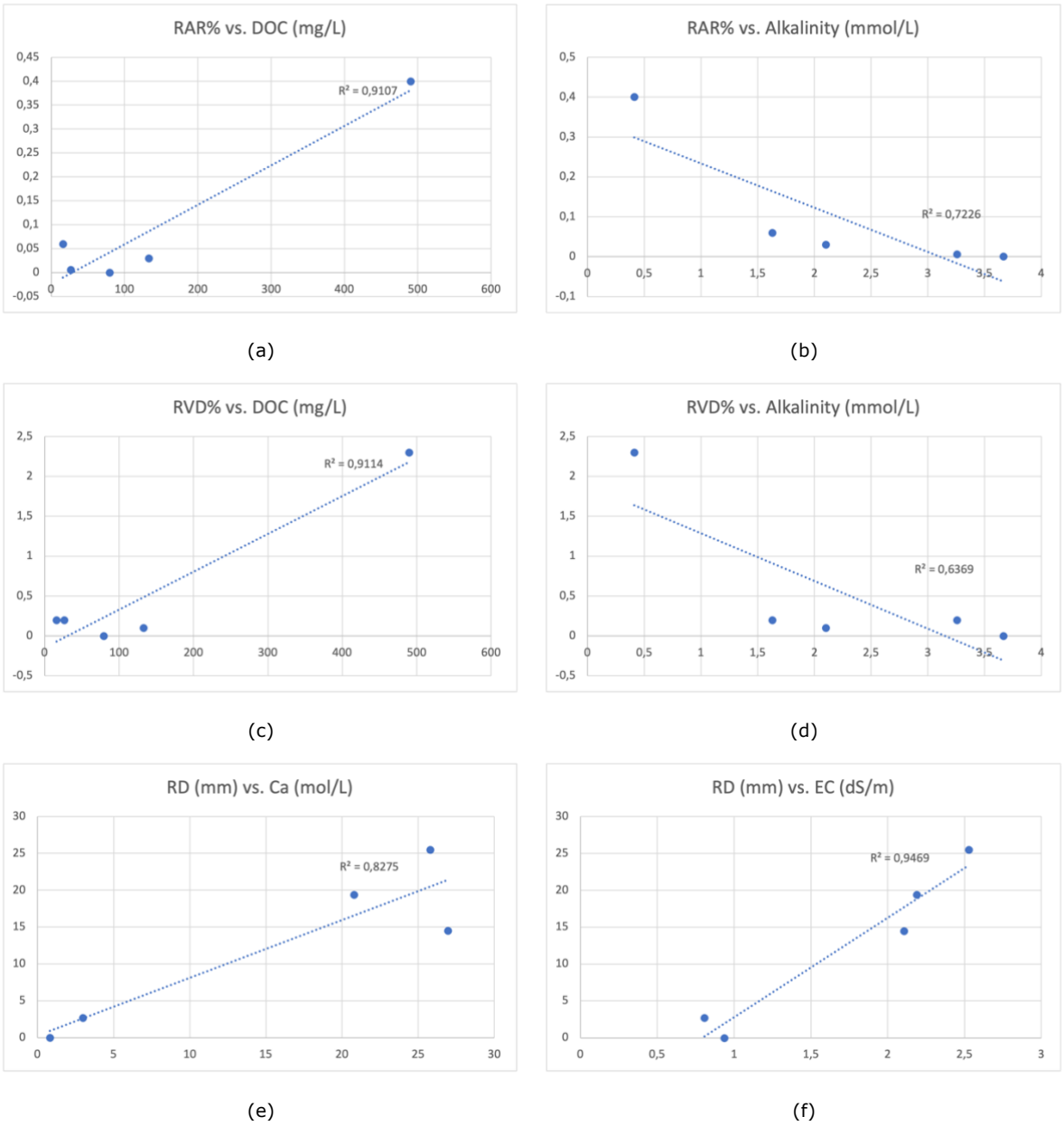

Figure 4-10. Correlations between chemical parameters and the measured root descriptors and the porosity. (a) RAR versus DOC with R-square value of 0.87, (b) RAR versus alkalinity with R-square value of 0.72, (c) RVD versus DOC with R-square value of 0.91, (d) RVD versus alkalinity with R-square value of 0.64, (e) RD versus Ca with R-square value of 0.83, and (f) RD versus EC with R-square value of 0.95.

5 Discussion

This section discusses the suitability of manual image segmentation for this study and examines the observed root architecture in different mixtures. Additionally, the mixtures are evaluated and ranked based on their effectiveness in supporting root growth. The relationship between the chemical characteristics, type of amendments, porosity of the mixtures, and their impact on root performance is also discussed.

5.1 Manual segmentation

The root segmentation process posed significant challenges and was found to be the most complex aspect of the image processing protocol in this study. For instance, the coarse parts of the acai waste adjacent to roots could be mistaken by root-developing seeds, even with the precision of human eye. This is apparent in Figure 4-5-b as sudden increase in RAR for the mixture containing acai seed waste at 15-20 mm depth. Likewise, the thin fibers around acai seeds could potentially be mis-segmented for hair roots.

Manual segmentation was extremely tedious yet the best fit for the purpose of this work. In other similar studies (Helliwell et al., 2017; Kemp et al., 2022), automated segmentation using machine learning was used. However, their pots (columns) had smaller diameters, 25 and 32 mm, while our column had the diameter of 50 mm which was more suitable to observe root´s spatial distribution (less 'pot-bound'). For this very fact, they could afford using much lower energy X-ray sources, voltage of 115 and 90 kV opposed to our voltage of 150 kV thus obtaining images with higher spatial contrast than ours. Another reason that we needed higher energy X-ray was that BR´s very high bulk density hinders the penetration of waves. Moreover, unlike the aforementioned studies where they focused on specific regions of interest in uniform soils, the quantification process in this study involved analyzing the entire bulk of a complex soil with more components to measure the root and soil features. The high energy X-ray source gave us the necessary spatial resolution such that we could see all components of our heterogenous samples while furnished us with less contrast resolution between roots, organic (acai or food) waste, and the BR, the conditions under which manual segmentation was a better option than automated alternatives.

5.2 Root architecture

When examining Figure 4-2 and Figure 4-6(-c and -d), it can be seen that BR90-G10 roots were dense and spread throughout the surface layer, with many small lateral roots and branching while BR85-G10-A5 and BR85-G10-A5 are growing mostly one-directionally along vertical axis of the column. The reason lies within the nutrition and water availability in the top layer as roots increase their branching in nutrient and water rich areas in the soil (Jin et al., 2017).

The dense soil below the top layer in BR90-G10 acted as a bed and limited the water passage to deep layers thus water was retained in the top layer and was utilized by roots. On the other hand, BR85-G10-A5 and BR85-G10-A5 owing to higher pore spaces at all depths, allowed both water passage and root elongation (Jin et al., 2013). As the water sank through the pores, the roots followed suit. The roots did not side-branch due to poor nutrition availability.

5.3 Root development and chemistry in BR

Table 5-1 summarizes the performance of each mixture according to the descriptors of the roots which was quantified using the methodology of this study.

Table 5-1. Performance summary of all mixtures in developing roots.

Mixture type[1]	Parameters to assess the performance pf ameliorated bauxite residue				
	RVD[2]	RD[3]	RAR[4]	No. of roots	#Cluster[5]
BR90-G10	☑	☑	☑	☑	2
BR90-G5-O5	☒	☒	☒	☒	0
BR90-G5-A5	☒	☒	☒	☒	0
BR85-G10-O5	☒	☑	☒	☒	~1
BR85-G10-A5	☑	☑	☑	☑	~2

Icons: good = ☑, decent = ☑, poor = ☒, worst = ☒

[1] BR = Bauxite residue, G = Gypsum, O = Organic food waste, A = Acai seed waste

[2] RVD = Root volume density, [3] RD = Root depth, [4] RAR = Root area ratio

[5] the cluster number to which each mixture belonged, after the principal component analysis of the chemical data at liquid to solid ratio of 10. ~ symbol means 'with the exception of one replicate'

Overall, the mixtures containing 10% gypsum showed varying levels of root growth while the mixtures containing 5% gypsum showed minimal to no root growth. This observation can potentially be explained by the significant difference (p value<0.05) between pH of mixtures with 10% gypsum (mean pH= 8.2) as compared to mixtures containing 5% gypsum (mean pH= 9), before seeding. This is not surprising as gypsum reduces pH by precipitating alkaline ions after introducing excess Ca^{2+}. The lower pH and less alkalinity favored the availability of essential nutrients, while concurrently limiting the presence of potentially toxic species like aluminate, eventually affecting the growth of the roots (Gräfe & Klauber, 2011; Gräfe et al., 2009; Xue et al., 2016). This was demonstrated by the negative correlation of RAR (R^2=0.72), and RVD (R^2=0.64) with the alkalinity of the mixtures (Figure 4-10-b and Figure 4-10-d).

The EC had the most pronounced effect on clustering of the samples. After the leaching, EC was significantly different (p value<0.05) between the mixtures containing 10% gypsum (mean EC= 2.3 dS m^{-1}) and the mixtures containing 5% gypsum (mean EC= 0.9 dS m^{-1}). All EC values met the rehabilitation goal of BR (EC< 4 dS m^{-1}) reported by (Di Carlo et al., 2019). This means at least water uptake by roots was not hindered due to reduced osmotic potential (Gräfe & Klauber, 2011), however the latter group had too low EC which can indicate nutritional deficiency (Ding et al., 2018). This effect of EC is demonstrated by its strong positive correlation (R^2=0.95) with the measured RD values in

this study which is shown in Figure 4-10-f. Indeed, the correlation has an upper limit for EC as increased levels of it is intolerable for plants.

Among 10 % gypsum mixtures, the one with no organic waste had the highest number of roots, highest RVD%, and highest average RAR% of 0.4% which exceeds the value reported by (De Baets et al., 2008) for another grass species grown in non-BR soil. They calculated a RAR of 0.08%, using root length per unit volume and root diameter information. The difference in methodology and the fact that root developing seeds in the first 10 mm of the soil were also included in our calculation explains the difference in measured values. The mixture with acai waste had highest RD among all and did slightly a better job in developing roots than the mixture with food waste. The same order of root performance per mixture observed in this study was reported in shoot performance in (Stubhaug, 2022), as it is shown in the appendix (Figure 10-2).

The SAR value of the leachate was the lowest in the treatment with only 10% gypsum, with mean of triplicate value of 6.1 which was 97% less than the pre-leaching value. This was within the rehabilitation goal of SAR<7 (Di Carlo et al., 2019). In this mixture, Na^+ was leached out effectively from the surface layer and its then-available exchange sites on BR particles were occupied by Ca^{2+}. It was observed in (Kong et al., 2018) that Na^+ migrates down the column rapidly with leaching while Ca^{2+} has stronger colloidal adsorption and migrates at lower rates. This is because the latter has higher charge density due to their lower atomic radius and higher valance number (Sparks, 2003). Likewise, (Bray et al., 2018) showed decrease of Na in the entire first 5 cm of their column and increase of Ca in the top 3 cm as a result of gypsum-OM treatment.

The reduction in leached Na^+ was due to either Na^+ being washed out of column during the leaching steps or being accumulated in the lower layers of column by adsorption to negatively charged particles. The accumulation of Na^+ in the lower depths caused dispersion thus soil compaction, which is evident by sharp decrease in porosity below the 15 mm depth of BR90-G10 (Figure 4-7-c).

Interestingly, the average RD for the mixture mentioned above was about the same as the depth at which porosity decreased sharply. It is difficult to say if the dense radial root growth (Figure 4-2-a, Figure 4-5) caused that compaction (Jin et al., 2013; Savioli et al., 2014), or the inherent consolidation and poor hydraulic conductivity of the soil, due to lack of organic matter (no organic waste amendment), excess of Na, etc., limited the root growth below that depth. Understanding this is out of the scope of this study but perhaps an estimation could be made by screening the compacted soil for root exudate chemicals. If there is found significant amounts of exudates in the compacted zone, it might indicate that the root growth is the cause, and the soil compaction the effect and not the other way around. It was observed by (Bardgett et al., 2014), that the root´s water uptake stimulated the reformation of clay, and that this microenvironment was rich in root mucilage.

5.3.1 With versus without organic waste

The fact that the 10% gypsum treatments with organic waste amendment had a poorer root performance in this study might seem counter-intuitive since the formers lower the pH more effectively and provide nutrition to plants through mineralization of organic matter. However, organic matter can enhance salinity, sodicity and toxicity levels in the

soil by introducing large amounts of salts, trace metals, and pathogens. Ongoing decomposition of organic matter when it is not adequately stabilized is another potential downside of organic amendments as it can lead to release of harmful chemicals or N immobilization in microorganism biomass. The N immobilization occurs when microorganisms utilize N to decompose C sources, rendering N unavailable for plant utilization (Leogrande & Vitti, 2018).

The columns in this study were vegetated right after the leaching test and before the organic matter and microbial community is sufficiently stabilized inside the mixture. Therefore, the organic matter was very labile with food waste being more labile than acai (food waste performed worse in hosting roots). Perhaps if there was a lag phase between the leaching and vegetation, or the organic wastes were pre-composted, better results could be expected. Moreover, anaerobic degradation of organic matter induced by decreasing porosity and thus decreased gas exchange rates, might have impeded the root growth by accumulating methane.

Al toxicity is a one of the barriers for vegetation in BR. Amendments with organic wastes introduced even more Al to the soil and despite the reduction in pH and alkalinity through leaching, the pH was still in the range where soluble specie of Al (aluminate) is dominant (Johan et al., 2021).

The mixture without organic waste as amendment had lower alkalinity after the leaching. This was probably caused by the contribution of organic matter to the total negative charge of the solution. The Ca^{+} ion introduced by gypsum, was bonded to the organic matter hence it was less available for precipitation of alkaline ions.

5.3.2 Acai versus food waste

The mixtures from 10% gypsum containing group which had developed less roots, differ only in the type of organic material, yet the difference in root performance between these two is considerable and a curious case. The BR85-G10-A5 hosted higher number of roots RAR, RVD and RD while BR85-G10-O5 showed a higher growth rate between the second and the fourth week.

Acai waste that was used in this study had noticeably lower EC, higher C/N (lower lability), lower Na content, Ca, and P as compared to the food waste Table 3-2. Apart from that, the acai waste had a coarser physical texture which could play a role in the slower rate of release of the carbon sources and at the same time it could increase the number of larger pore spaces leading to better hydraulic conductivity. In (Stubhaug, 2022), it was observed that the color of the leachates from these two mixtures were different initially in the leaching process (at lower L/S´s), however the difference reduced as L/S increased. Stubhaug (2022) concluded that food waste supplied effectively more labile organic C as compared to acai waste. This suggests that the energy sources from food waste were decomposed by microorganisms before the plants could use them in long-term.

5.4 Root development and porosity in BR

The porosity in general had decreased with time across all mixtures. In contrast, (Helliwell et al., 2017) who also used micro-CT to assess physical changes in rhizosphere had concluded that the porosity of rhizosphere had increased in the clay loam which is close to BR (silty clay). However, they had investigated the soil only 0.024 mm and 0.600 mm

away from the root whereas in this study the average porosity of the whole area (r=25 mm) of the column horizontal cross-sections, showed the decrease. On the contrary, (Kemp et al., 2022) found that the void ratio decreased as a result of root growth as they looked into a larger 'regions of interest' (r=3.5, 7.1, 10.6, 14.1 mm), which in agreement with the observation made in this study. In both abovementioned studies it was concluded that root growth does influence the porosity and void ratio of the soil which is in line with our results in which i) the decrease in porosity was first evident in the top layer where roots were starting to grow and then it was expanded to lower layers Figure 4-7, and ii) the mixtures with 10% gypsum (root-developing ones) showed higher STD in porosity values after four weeks of growth (Table 4-1).

In a recent international workshop about root-soil-atmosphere interactions, it was concluded that based on studies done so far in natural soils, vegetation tends to decrease porosity in loose soils and increase the porosity in fine-dense soils (Capobianco, 2023). In BR from Alunorte (silty clay) used in this study, we are seeing the opposite. The porosity is decreasing which leads to lower water infiltration and gas exchange rates therefore not favorable for the roots. The ability of the roots to increase porosity by expanding the already-existing pores or 'negotiating' new ones was outcompeted by the extreme physical and chemical conditions of BR.

Porosity calculated by different RS researchers using CT imaging is somewhere between 13% and 73% depending on the experimental conditions such as type of soil, plant species, timespan of growth, among others (Hou et al., 2022). The porosities of amended BR in this study before the vegetation was 62-65 % and is in agreement with non-image-based quantified porosities that was reported by (Courtney et al., 2013) from the gypsum-compost amended BR which was 64.3%. This shows the accuracy of the algorithmic method used in this study based on CT imaging for measuring porosity.

6 Conclusion

The analysis of root systems using image processing techniques on non-destructively and sequentially acquired μCT scans from structurally complex ameliorated bauxite residue was shown to be a precise and effective method. Root development was closely linked to the enhanced physical and chemical characteristics of the residue caused by leaching and amendments.

The optimized μCT operating parameters were crucial in providing the best spatial and contrast resolution for the complex mixtures. Due to complexity of the samples, manual root segmentation was utilized to identify root material. From the visual inspection of segmented roots, the superiority of the three mixtures with 10% gypsum in developing roots was already established. Through a series of algorithmic steps on the segmented roots and visualizations, it was possible to further quantify the differences between those three mixtures.

The mixture with 10% gypsum showed the best performance in developing roots. It was followed by the mixture with 10% gypsum and 5% acai seed waste with considerably smaller number of roots and lower root volume density and root area ratio. Lastly, the mixture with 10% gypsum and 5% food waste showed some root growth and the highest growth rate during the second two weeks of growth. The difference in root performance between the mixtures with 10% gypsum and %5 acai/food waste stems from the lability levels of their organic carbon sources as well as release rate of those sources which is closely related to their physical form.

There was a considerable variability in porosity of the mixtures with time, but the general trend was decrease in porosity. This was shown to be related with the root growth and the composition of the mixtures.

The results from latent variable analysis followed by clustering analysis of the chemical data of the mixtures partially accounted for the link between chemical states of the mixtures and their ability to accommodate root growth. The electrical conductivity was the parameter which explained most of the variability within the chemical data and was strongly correlated with root depth.

This study, by focusing on root growth, showed that weight proportion of gypsum and type of organic amendments are important for an optimal long-term revegetation strategy. The leaching process as an important factor in lowering the hostility of bauxite residue for plants might be less effective under field conditions if high-electrolyte water is used. This bio-rehabilitation strategy is the best option at hand to mitigate environmental impacts of alumina refinery on both global and local scales.

7 Future work

7.1.1 Digital counting of metals

It is possible to construct an algorithm for the depth-based quantification of total metal containing particles, which are mainly Fe and Al, in BR by using a very similar approach that was employed for RAR% and porosity%. The metals are the densest particles in the BR and appear bright (greyscale intensities close to 256) so it is possible to effectively threshold-out and quantify the metal levels. An estimation of Fe content in BR can be used to compare samples at different L/S in the context of Fe´s leaching behavior. It could also be used before and after a revegetation trial to measure plants uptake of metals. Beside the research community, this can have applications for aluminum industry as for continuous, nimble, and non-destructive monitoring of the BRDA.

7.1.2 Root diameter measurement

Root diameter can be considered as a measure of root's influence on mechanical properties of the soil which is important in targeted applications of roots for example in bio-engineered slopes. A way to approach this is to isolate individual roots (regions of interests) in the segmented volume or only segmenting individual roots in the first place and then define algorithmic steps for measuring diameter along the root´s own axis or its penetrated depth.

9 References

Alunorte&EcoForest. *Evaluation of different revegetation techniques in Solid Waste Deposit - DRS refinery Alunorte.*

Ashkenazi, D. (2019). How aluminum changed the world: A metallurgical revolution through technological and cultural perspectives. *Technological Forecasting and Social Change*, *143*, 101-113. https://doi.org/https://doi.org/10.1016/j.techfore.2019.03.011

Bardgett, R. D., Mommer, L., & De Vries, F. T. (2014). Going underground: root traits as drivers of ecosystem processes. *Trends Ecol Evol*, *29*(12), 692-699. https://doi.org/10.1016/j.tree.2014.10.006

Boas, F., & Fleischmann, D. (2012). CT artifacts: Causes and reduction techniques. *Imaging in Medicine*, *4*. https://doi.org/10.2217/iim.12.13

Bray, A. W., Stewart, D. I., Courtney, R., Rout, S. P., Humphreys, P. N., Mayes, W. M., & Burke, I. T. (2018). Sustained Bauxite Residue Rehabilitation with Gypsum and Organic Matter 16 years after Initial Treatment. *Environmental Science & Technology*, *52*(1), 152-161. https://doi.org/10.1021/acs.est.7b03568

Canarini, A., Kaiser, C., Merchant, A., Richter, A., & Wanek, W. (2019). Root Exudation of Primary Metabolites: Mechanisms and Their Roles in Plant Responses to Environmental Stimuli. *Front Plant Sci*, *10*, 157. https://doi.org/10.3389/fpls.2019.00157

Capobianco, V. (2023). Personal Correspondance. In.

Cormack, A. M. (1963). Representation of a Function by Its Line Integrals, with Some Radiological Applications. *Journal of Applied Physics*, *34*(9), 2722-2727. https://doi.org/10.1063/1.1729798

Courtney, R., Harrington, T., & Byrne, K. A. (2013). Indicators of soil formation in restored bauxite residues. *Ecological Engineering*, *58*, 63-68. https://doi.org/https://doi.org/10.1016/j.ecoleng.2013.06.022

Courtney, R., & Mullen, G. (2009-b). Use of Germination and Seedling Performance Bioassays for Assessing Revegetation Strategies on Bauxite Residue. *Water, Air, and Soil Pollution*, *197*(1), 15-22. https://doi.org/10.1007/s11270-008-9787-8

Courtney, R., Mullen, G., & Harrington, T. (2009-a). An Evaluation of Revegetation Success on Bauxite Residue. *Restoration Ecology*, *17*(3), 350-358. https://doi.org/https://doi.org/10.1111/j.1526-100X.2008.00375.x

De Baets, S., Poesen, J., Reubens, B., Wemans, K., De Baerdemaeker, J., & Muys, B. (2008). Root tensile strength and root distribution of typical Mediterranean plant species and their contribution to soil shear strength. *Plant and Soil*, *305*(1), 207-226. https://doi.org/10.1007/s11104-008-9553-0

Di Carlo, E., Boullemant, A., & Courtney, R. (2020). Ecotoxicological risk assessment of revegetated bauxite residue: Implications for future rehabilitation programmes. *Sci Total Environ*, *698*, 134344. https://doi.org/10.1016/j.scitotenv.2019.134344

Di Carlo, E., Chen, C. R., Haynes, R. J., Phillips, I. R., & Courtney, R. (2019). Soil quality and vegetation performance indicators for sustainable rehabilitation of bauxite residue disposal areas: a review. *Soil Research*.

Ding, X., Jiang, Y., Zhao, H., Guo, D., He, L., Liu, F., Zhou, Q., Nandwani, D., Hui, D., & Yu, J. (2018). Electrical conductivity of nutrient solution influenced photosynthesis, quality, and antioxidant enzyme activity of pakchoi (Brassica campestris L. ssp. Chinensis) in a

hydroponic system. *PLoS One*, *13*(8), e0202090. https://doi.org/10.1371/journal.pone.0202090

Dursun, T., & Soutis, C. (2014). Recent developments in advanced aircraft aluminium alloys. *Materials & Design (1980-2015)*, *56*, 862-871. https://doi.org/https://doi.org/10.1016/j.matdes.2013.12.002

Foresta, V., Capobianco, V., & Cascini, L. (2020). Influence of grass roots on shear strength of pyroclastic soils. *Canadian Geotechnical Journal*, *57*(9), 1320-1334. https://doi.org/10.1139/cgj-2019-0142

Fourrier, C., Luglia, M., Keller, C., Hennebert, P., Foulon, J., Ambrosi, J.-P., Angeletti, B., & Criquet, S. (2021). How Raw and Gypsum Modified Bauxite Residues Affect Seed Germination, Enzyme Activities, and Root Development of Sinapis alba. *Water, Air, & Soil Pollution*, *232*(8), 309. https://doi.org/10.1007/s11270-021-05232-x

Gostick, J., Khan, Z. A., Tranter, T., Kok, M., Agnaou, M., Sadeghi, M., & Jervis, R. (2019). PoreSpy: A Python Toolkit for Quantitative Analysis of Porous Media Images. *Journal of Open Source Software*, *4*, 1296. https://doi.org/10.21105/joss.01296

Gräfe, M., & Klauber, C. (2011). Bauxite residue issues: IV. Old obstacles and new pathways for in situ residue bioremediation. *Hydrometallurgy*, *108*(1), 46-59. https://doi.org/https://doi.org/10.1016/j.hydromet.2011.02.005

Gräfe, M., Power, G., & Klauber, C. (2009). Review of Bauxite Residue Alkalinity and Associated Chemistry.

Hainsworth, J., & Aylmore, L. (1983). The use of computer assisted tomography to determine spatial distribution of soil water content. *Soil Research*, *21*(4), 435-443. https://doi.org/https://doi.org/10.1071/SR9830435

Helliwell, J. R., Sturrock, C. J., Mairhofer, S., Craigon, J., Ashton, R. W., Miller, A. J., Whalley, W. R., & Mooney, S. J. (2017). The emergent rhizosphere: imaging the development of the porous architecture at the root-soil interface. *Scientific Reports*, *7*(1), 14875. https://doi.org/10.1038/s41598-017-14904-w

Hou, L., Gao, W., der Bom, F., Weng, Z., Doolette, C. L., Maksimenko, A., Hausermann, D., Zheng, Y., Tang, C., Lombi, E., & Kopittke, P. M. (2022). Use of X-ray tomography for examining root architecture in soils. *Geoderma*, *405*, 115405. https://doi.org/https://doi.org/10.1016/j.geoderma.2021.115405

Hounsfield, G. N. (1973). Computerized transverse axial scanning (tomography). 1. Description of system. *Br J Radiol*, *46*(552), 1016-1022. https://doi.org/10.1259/0007-1285-46-552-1016

Hydro. (2019). *Sustainability report for Hydro's operations in Brazil 2018*.

Jin, K., Shen, J., Ashton, R. W., Dodd, I. C., Parry, M. A. J., & Whalley, W. R. (2013). How do roots elongate in a structured soil? *Journal of Experimental Botany*, *64*(15), 4761-4777. https://doi.org/10.1093/jxb/ert286

Jin, K., White, P. J., Whalley, W. R., Shen, J., & Shi, L. (2017). Shaping an Optimal Soil by Root–Soil Interaction. *Trends in Plant Science*, *22*(10), 823-829. https://doi.org/https://doi.org/10.1016/j.tplants.2017.07.008

Johan, P. D., Ahmed, O., Omar, L., & Hasbullah, A. (2021). Phosphorus Transformation in Soils Following Co-Application of Charcoal and Wood Ash. *Agronomy*, *11*, 2010. https://doi.org/10.3390/agronomy11102010

Jones, B. E. H., & Haynes, R. J. (2011). Bauxite Processing Residue: A Critical Review of Its Formation, Properties, Storage, and Revegetation. *Critical Reviews in Environmental*

Science and Technology, *41*(3), 271-315. https://doi.org/10.1080/10643380902800000

Jones, B. E. H., Haynes, R. J., & Phillips, I. R. (2012). Addition of an organic amendment and/or residue mud to bauxite residue sand in order to improve its properties as a growth medium. *Journal of Environmental Management*, *95*(1), 29-38. https://doi.org/https://doi.org/10.1016/j.jenvman.2011.09.014

Kemp, N., Angelidakis, V., Luli, S., & Nadimi, S. (2022). How Do Roots Interact with Layered Soils? *Journal of Imaging*, *8*(1), 5. https://www.mdpi.com/2313-433X/8/1/5

Kong, X.-f., Jiang, X.-x., Xue, S.-g., Huang, L., Hartley, W., Wu, C., & Li, X.-f. (2018). Migration and distribution of saline ions in bauxite residue during water leaching. *Transactions of Nonferrous Metals Society of China*, *28*(3), 534-541. https://doi.org/https://doi.org/10.1016/S1003-6326(18)64686-2

Lehoux, A. P., Lockwood, C. L., Mayes, W. M., Stewart, D. I., Mortimer, R. J. G., Gruiz, K., & Burke, I. T. (2013). Gypsum addition to soils contaminated by red mud: implications for aluminium, arsenic, molybdenum and vanadium solubility. *Environmental Geochemistry and Health*, *35*(5), 643-656. https://doi.org/10.1007/s10653-013-9547-6

Leogrande, R., & Vitti, C. (2018). Use of organic amendments to reclaim saline and sodic soils: a review. *Arid Land Research and Management*, *33*, 1-21. https://doi.org/10.1080/15324982.2018.1498038

Lervik, A. (2023). *Chemometrics KJ8175 course material* Norwegian University of Science and Technology.

Mooney, S. J., Pridmore, T. P., Helliwell, J., & Bennett, M. J. (2012). Developing X-ray Computed Tomography to non-invasively image 3-D root systems architecture in soil. *Plant and Soil*, *352*(1), 1-22. https://doi.org/10.1007/s11104-011-1039-9

Ortiz, J. F. T. (2021). *Bauxite Residue Disposal and the Environmental Benefit of Açaí, Soil and Gypsum Amendments* University of Oslo]. Oslo, Norway.

Petrovic, A. M., Siebert, J. E., & Rieke, P. E. (1982). Soil Bulk Density Analysis in Three Dimensions by Computed Tomographic Scanning. *Soil Science Society of America Journal*, *46*(3), 445-450. https://doi.org/https://doi.org/10.2136/sssaj1982.03615995004600030001x

Pires, L. F., Borges, J. A. R., Bacchi, O. O. S., & Reichardt, K. (2010). Twenty-five years of computed tomography in soil physics: A literature review of the Brazilian contribution. *Soil and Tillage Research*, *110*(2), 197-210. https://doi.org/https://doi.org/10.1016/j.still.2010.07.013

Saltzman, W. M. (2009). *Biomedical engineering : bridging medicine and technology*. Cambridge University Press. p 432-442.

Savioli, A., Viggiani, C., & Santamarina, J. C. (2014). Root-Soil Mechanical Interaction. In *Geo-Congress 2014 Technical Papers* (pp. 3977-3984). https://doi.org/doi:10.1061/9780784413272.386

Schneider, J. (2020). *Mineralogical and Geotechnical Characterization of Bauxite Residue A case study from NE Brazil* UNIVERSITY OF OSLO]. Oslo, Norway.

scikit-learn. (2023). scikit-learn developers (BSD License). Retrieved 21.04.2023 from https://scikit-learn.org/stable/modules/decomposition.html#decompositions

Sparks, D. L. (2003). *Environmental soil chemistry* (2nd ed.). Academic Press. p 285-300.

statista. (2022). *Bauxite mine production in Brazil in 2020, by state*. Retrieved 03.2023 from https://www.statista.com/statistics/1025772/brazil-bauxite-mine-production-state/

Stubhaug, H. P. (2022). *Cation exchange capacity, and amendment effect of gypsum and organic matter on chemical properties and aggregate stability of bauxite residue* Norwegian University of Life Sciences]. Ås, Norway.

Swain, B., Lee, C. G., & Park, J. R. (2022). Assessment of bauxite residue as secondary resource for rare earth metal and valorization challenges: A perspective. *Resources, Conservation & Recycling Advances*, *14*, 200078. https://doi.org/https://doi.org/10.1016/j.rcradv.2022.200078

Taina, I. A., Heck, R. J., & Elliot, T. R. (2008). Application of X-ray computed tomography to soil science: A literature review. *Canadian Journal of Soil Science*, *88*(1), 1-19. https://doi.org/10.4141/cjss06027

V. S. Quinteros, V. C., H. Stubhaug, G. Okkenhaug, C. Berge Hansen, Y. Silveira Miura, P. Chutigan and J. Mulder. (2023). *Bauxite residue tailings amelioration and revegetation: roots growth assessment using mCT-scanning and image analysis.* [Proceedings of the 9th International Congress on Environmental Geotechnics, 25-28 June, 2023, Chania, Greece. In print.].

Wik, S. A. (2020). *Mobility of Chemical Elements in Bauxite Residue A case study from NE Brazil*

University of Oslo]. Oslo, Norway.

Wildenschild, D., Vaz, C. M. P., Rivers, M. L., Rikard, D., & Christensen, B. S. B. (2002). Using X-ray computed tomography in hydrology: systems, resolutions, and limitations. *Journal of Hydrology*, *267*(3), 285-297. https://doi.org/https://doi.org/10.1016/S0022-1694(02)00157-9

Wong, J. W. C., & Ho, G. (1994). Sewage sludge as organic ameliorant for revegetation of fine bauxite refining residue. *Resources, Conservation and Recycling*, *11*(1), 297-309. https://doi.org/https://doi.org/10.1016/0921-3449(94)90097-3

Wong, J. W. C., & Ho, G. E. (1993). Use Of Waste Gypsum In The Revegetation On Red Mud Deposits: A Greenhouse Study. *Waste Management & Research*, *11*(3), 249-256. https://doi.org/https://doi.org/10.1006/wmre.1993.1024

Xue, S., Zhu, F., Kong, X., Wu, C., Huang, L., Huang, N., & Hartley, W. (2016). A review of the characterization and revegetation of bauxite residues (Red mud). *Environmental Science and Pollution Research*, *23*(2), 1120-1132. https://doi.org/10.1007/s11356-015-4558-8

Yushkevich, P. A., Piven, J., Hazlett, H. C., Smith, R. G., Ho, S., Gee, J. C., & Gerig, G. (2006). User-guided 3D active contour segmentation of anatomical structures: significantly improved efficiency and reliability. *Neuroimage*, *31*(3), 1116-1128. https://doi.org/10.1016/j.neuroimage.2006.01.015

Zhang, J., Song, B., Wei, Q., Bourell, D., & Shi, Y. (2019). A review of selective laser melting of aluminum alloys: Processing, microstructure, property and developing trends. *Journal of Materials Science & Technology*, *35*(2), 270-284. https://doi.org/https://doi.org/10.1016/j.jmst.2018.09.004

Zhu, F., Liao, J., Xue, S., Hartley, W., Zou, Q., & Wu, H. (2016). Evaluation of aggregate microstructures following natural regeneration in bauxite residue as characterized by synchrotron-based X-ray micro-computed tomography. *Sci Total Environ*, *573*, 155-163. https://doi.org/10.1016/j.scitotenv.2016.08.108

10 Appendix

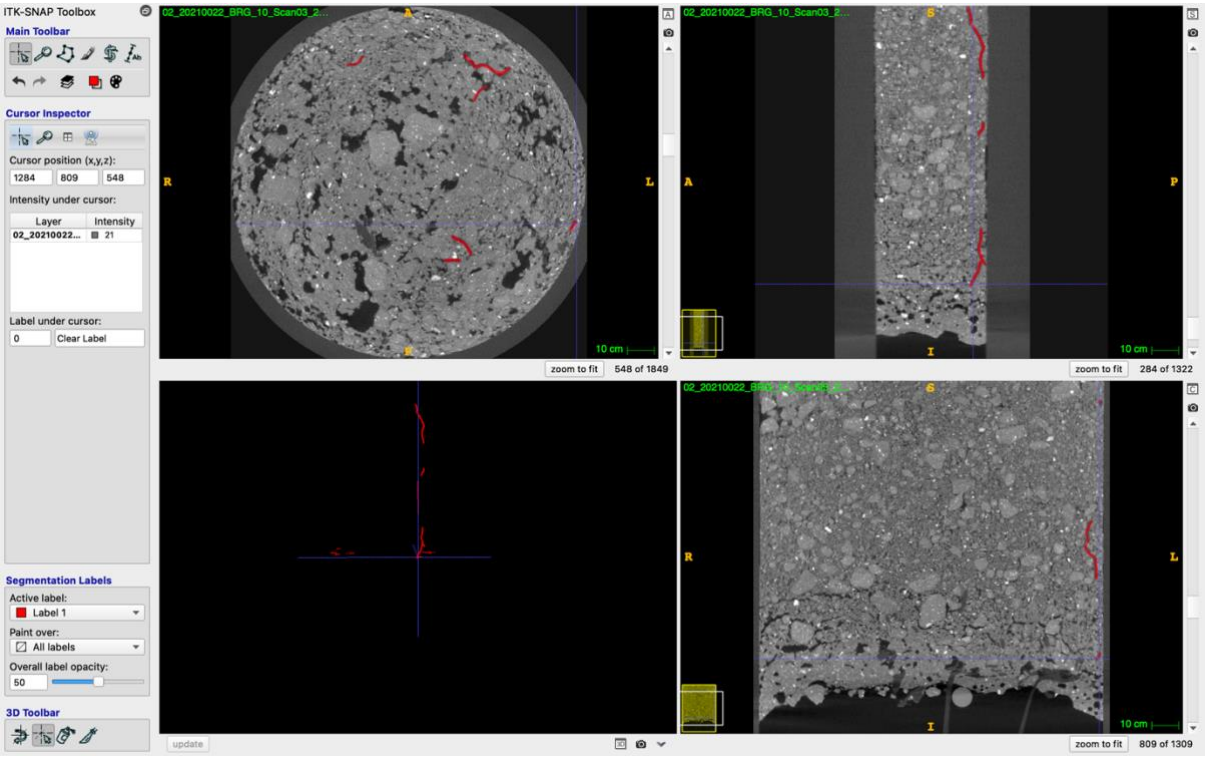

Figure 10-1. ITK-SNAP interface

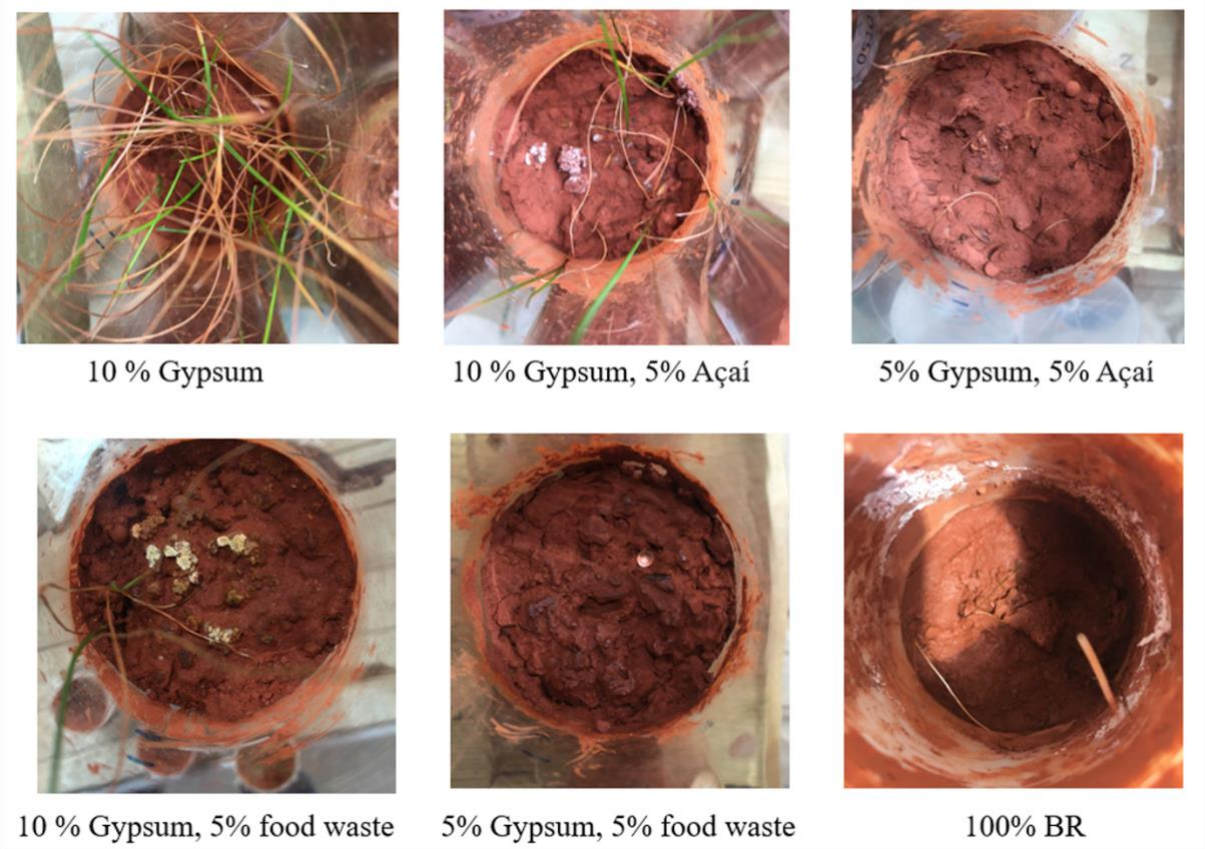

Figure 10-2. Visual observation of the shoot growth. From (Stubhaug, 2022).

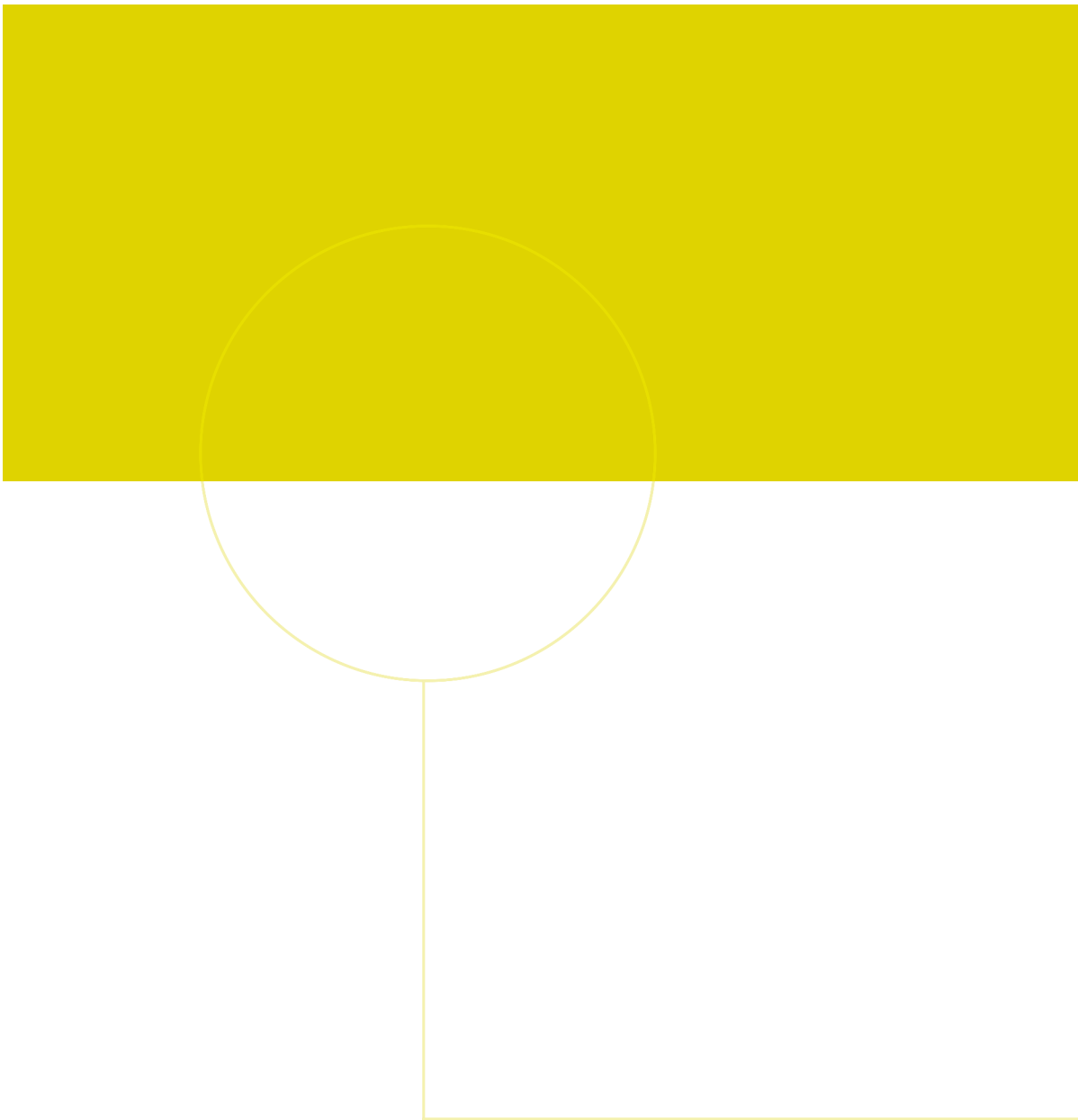

NTNU
Norwegian University of
Science and Technology

NGI